FLAVOR PROPAGATIONS OF HIGH ENERGY COSMIC NEUTRINOS

By

Lingjun Fu

Dissertation

Submitted to the Faculty of the

Graduate School of Vanderbilt University

in partial fulfillment of the requirements

for the degree of

DOCTOR OF PHILOSOPHY

in

PHYSICS

May, 2017

Nashville, TN

Approved:

Thomas J. Weiler, Ph.D.

Kelly Holley-Bockelmann, Ph.D.

Thomas W. Kephart, Ph.D.

Paul D. Sheldon, Ph.D.

Julia Velkovska, Ph.D.

ACKNOWLEDGMENTS

I would like to thank Dr. Thomas Weiler and Dr. Thomas Kephart for the unforgettable experience at Vanderbilt. This thesis would be impossible without their help. Dr. Weiler deserves specially appreciation for his full support of my career development.

Special thanks are due to the other wonderful members of my Ph.D. committee: Dr. Kelly Holley-Bockelmann, Dr. Paul Sheldon, and Dr. Julia Velkovska. Their invaluable services in the committee and expertise in physics help to improve this work.

Dr. Chiu Man Ho and Dr. Yonghui Li have shared their insights with me in countless discussions of both physics and programming. This work has benefited from the collaborations with them as well.

I would also thank all my friends at Vanderbilt for the uncountable moments when we share the happiness and sorrow with each other.

My wife, Xianwen Shen, has always been my source of support, motivation, and backup during this warm and touching journey. Without her, my life would get stuck and I could never become who I am now.

Finally, this work is specially dedicated to my parents, who have sacrificed so much to offer me the best opportunities.

TABLE OF CONTENTS

LIST OF TABLES

LIST OF FIGURES

CHAPTER I

Introduction

I.1 Histories of Neutrinos

The history of neutrinos, the knowledge of cosmic neutrinos and the discovery of neutrino properties, is a proud one for both theoretical and experimental physicists. The idea of neutrino was put forward by W. Pauli in 1930. After that, it was established in the Ellis and Wooster experiment that the average energy of the electrons produced in the β-decay is significantly smaller than the total released energy. Only the existence of a neutral particle with a small mass, which is emitted in the β-decay together with the electron, could save the fundamental law of conservation of energy. That particle, is called "neutrino".

We now know that the twelve fundamental fermions exist in nature: six quarks u, d, c, s, t, b, three charged leptons e, μ, τ and three neutrinos ν_e, ν_μ, ν_τ. In the Lagrangian of the electroweak interactions, neutrinos enter on the same footings as the quarks and the charged leptons. There are two basic differences between neutrinos and other fundamental fermions.

- At all available energies, cross section of the interaction of neutrinos with matter is many order of magnitude smaller than the one of the electromagnetic interaction of leptons with matter.

- Neutrino masses are many order of the magnitude smaller than the masses of leptons and quarks. However, neutrino is not massless, as a necessary requirement of neutrino oscillation data.

The Standard Model (SM) describes nearly all existing experimental data. However, existence of Dark Matter and other problems such as hierarchy problem implicates a theory beyond the SM. The first signature of new, beyond the SM physics was observed in the neutrino oscillation experiments. It is a common opinion that a new mechanism of the

mass generation is required. A quantum mechanical explanation is: flavor neutrino states are connected with states of neutrinos with definite masses by the unitary mixing matrix which is characterized by three mixing angles and one phase. This phenomenon is similar to the well established quark mixing. However, the quark mixing angles are small and satisfy a hierarchy. The neutrino mixing angles are completely different with two large angles and one small one. On the other hand, the most common general explanation of the smallness of the neutrino mass is based on the assumption of lepton number violation. If this assumption is correct, neutrinos are truly Majorana particles. As the investigation of neutrinos is entering a new precision era, the main problems which will be addressed ate the following

- Are neutrinos with definite masses Majorana or Dirac particles?
- What is the value of the smallest mixing angle θ_{13}?
- Is *CP* invariance violated in the lepton sector? What is the value of the *CP* phase?
- What is the mass scale and mass hierarchy of neutrinos? Is it normal or inverted?
- Does the sterile neutrino exist or not?

Perhaps the most exciting and significant experiment in neutrino physics in the 20th century is the measurement of neutrinos from the solar core as a way to probe the Sun and the intrinsic properties of neutrinos. The most numerous are those from the primary *PP* reaction. Many terrestrial and astrophysical neutrino experiments of the next generation have started or been proposed to start soon. New large detectors of atmospheric, solar and supernova neutrinos are under development. Technologies for new neutrino facilities (Super-beam, β-beam, Neutrino Factory) are being developed. There is no doubt that a new exciting era of neutrino physics is ahead.

I.2 Neutrinos in Astrophysics and Cosmology

The development of neutrino physics is intimately linked to theoretical studies of the Sun. The Sun is a star going through the Main Sequence phase, the most stable and long evolutionary phase, where stars consume the hydrogen in their cores. Detecting solar neutrinos seemed, in the 1960s, a good astrophysics experiment to test stellar structure and evolution theories. Solar neutrino predictions from Standard Solar Models (SSM) calculations have been extensively used to help constraining neutrino parameters such as mixing angles and mass splitting. Most spectacular and unexpected were the neutrino fireworks (in the 10 MeV range) from Supernova 1987A, which revealed the only neutrino source beyond our solar system until the discovery at IceCube. IceCube is a particle detector at the South Pole that records the interactions of neutrinos. In 1998 Super-Kamiokande went on to confirm the long-suspected neutrino oscillation phenomenon via muon neutrinos produced in the atmosphere.

The broad role of neutrinos as radiation is possible because of their small masses. Actually, in a typical stellar plasma or in the early universe, the dispersive photon mass far exceeds that of neutrinos, allowing for the plasma decay process $\gamma \to \nu\bar{\nu}$. Of course, neutrinos do have small vacuum masses and therefore contribute a small fraction of the cosmic dark matter. Moreover, their small masses may be responsible for creating the cosmic matter-antimatter asymmetry by virtue of the leptogenesis mechanism.

The second bread role of neutrinos is that of astrophysical messengers. Neutrinos can reach us from sites that are opaque to photons, in particular from the interior of the Sun and of core-collapse supernovae. It may even become possible to study the Earth's crust and interior by observing the geophysical $\bar{\nu}_e$ flux from natural radioactive elements. High-energy neutrinos that are produced in the context of cosmic-ray acceleration and propagation may become observable in future large-scale neutrino telescopes. The reason roots in the fact that electric charge neutrality prevents neutrino deflection in galactic and intergalactic magnetic fields (ignoring its own small magnetic moment) so that they point back

to their sources, in contrast to nuclei and protons, hopefully allowing one to identify the mysterious cosmic-ray accelerators.

Finally, one may use the "heavenly laboratories" to learn about the properties of neutrinos themselves such as oscillation parameters and overall mass scale. In addition, astrophysical and cosmological arguments constrain a broad range of non-standard neutrino properties such as electromagnetic form factors, secret interactions, or numbers and properties of sterile neutrinos. Note that light massive neutrinos could also play a role in the generation of the baryon asymmetry of the Universe from a preciously created lepton asymmetry. Respectively, one can also obtain quite restrictive bounds on light neutrino masses, which are however model-dependent. The existence of a relic sea of neutrinos is a generic feature of the standard hot big bang model. The number of neutrinos is only slightly below that of relic photons that constitute the cosmic microwave background (CMB). This cosmic neutrino background (CNB) has not been detected yet, but its presence is indirectly established by the accurate agreement between the calculated and observed primordial abundances of light elements.

I.3 Neutrino Masses and Mixings Phenomenology

Considering possible neutrino mass terms, the total Lagrangian has a term where the flavor fields enter into the interaction Lagrangian of the Standard Model. Neutrino flavor states are linear superpositions of the different mass eigenstates. given N flavors of neutrinos, there are N neutrino mass eigenstates, and mixing is parameterized by a unitary $N \times N$ matrix, U. Generally this mixing is given by

$$|\nu_\alpha\rangle = \sum_i U^*_{\alpha i} |\nu_i\rangle$$

where U is parameterized by $N(N-1)/2$ mixing angles and up to $N(N+1)/2$ phases given N neutrino flavors. In the case of $N = 3$, the matrix U is named as Pontecorvo-Maki-Nakagawa-Sakata (PMNS) matrix after four famous physicists. The latest global best fits

of the mixing parameters can be found in [1] as shown in Figure I.1. The PMNS matrix can be written as:

$$\begin{bmatrix} c_{12}c_{13} & s_{12}c_{13} & s_{13}e^{-i\delta} \\ -s_{12}c_{23} - c_{12}s_{23}s_{13}e^{i\delta} & c_{12}c_{23} - s_{12}s_{23}s_{13}e^{i\delta} & s_{23}c_{13} \\ s_{12}s_{23} - c_{12}c_{23}s_{13}e^{i\delta} & -c_{12}s_{23} - s_{12}c_{23}s_{13}e^{i\delta} & c_{23}c_{13} \end{bmatrix} \tag{I.1}$$

where s_{ij} and c_{ij} are used to denote $\sin\theta_{ij}$ and $\cos\theta_{ij}$ respectively with subscripts denoting the three planes of rotation in 3 dimensional space.

NuFIT 2.0 (2014)

	Normal Ordering ($\Delta\chi^2 = 0.97$)		Inverted Ordering (best fit)		Any Ordering
	bfp $\pm 1\sigma$	3σ range	bfp $\pm 1\sigma$	3σ range	3σ range
$\sin^2\theta_{12}$	$0.304^{+0.013}_{-0.012}$	$0.270 \to 0.344$	$0.304^{+0.013}_{-0.012}$	$0.270 \to 0.344$	$0.270 \to 0.344$
$\theta_{12}/^\circ$	$33.48^{+0.78}_{-0.75}$	$31.29 \to 35.91$	$33.48^{+0.78}_{-0.75}$	$31.29 \to 35.91$	$31.29 \to 35.91$
$\sin^2\theta_{23}$	$0.452^{+0.052}_{-0.028}$	$0.382 \to 0.643$	$0.579^{+0.025}_{-0.037}$	$0.389 \to 0.644$	$0.385 \to 0.644$
$\theta_{23}/^\circ$	$42.3^{+3.0}_{-1.6}$	$38.2 \to 53.3$	$49.5^{+1.5}_{-2.2}$	$38.6 \to 53.3$	$38.3 \to 53.3$
$\sin^2\theta_{13}$	$0.0218^{+0.0010}_{-0.0010}$	$0.0186 \to 0.0250$	$0.0219^{+0.0011}_{-0.0010}$	$0.0188 \to 0.0251$	$0.0188 \to 0.0251$
$\theta_{13}/^\circ$	$8.50^{+0.20}_{-0.21}$	$7.85 \to 9.10$	$8.51^{+0.20}_{-0.21}$	$7.87 \to 9.11$	$7.87 \to 9.11$
$\delta_{\rm CP}/^\circ$	306^{+39}_{-70}	$0 \to 360$	254^{+63}_{-62}	$0 \to 360$	$0 \to 360$
$\frac{\Delta m^2_{21}}{10^{-5}\ \mathrm{eV}^2}$	$7.50^{+0.19}_{-0.17}$	$7.02 \to 8.09$	$7.50^{+0.19}_{-0.17}$	$7.02 \to 8.09$	$7.02 \to 8.09$
$\frac{\Delta m^2_{3\ell}}{10^{-3}\ \mathrm{eV}^2}$	$+2.457^{+0.047}_{-0.047}$	$+2.317 \to +2.607$	$-2.449^{+0.048}_{-0.047}$	$-2.590 \to -2.307$	$\begin{bmatrix} +2.325 \to +2.599 \\ -2.590 \to -2.307 \end{bmatrix}$

Figure I.1: Global best fit ranges of neutrino mixing parameters

One can compute oscillation probabilities for the process $\nu_\alpha \to \nu_\beta$, which depend on the neutrino energy as well as the propagation length. They are given by

$$\begin{aligned} P_{\alpha\beta}(L/E) =& \delta_{\alpha\beta} - 4\sum_{i>j} \mathrm{Re}(U^*_{\alpha i}U_{\beta i}U^*_{\beta j}U_{\alpha j}) \sin^2\left(\frac{\Delta m^2_{ij}L}{4E}\right) \\ &+ 2\sum_{i>j} \mathrm{Im}(U^*_{\alpha i}U_{\beta i}U^*_{\beta j}U_{\alpha j}) \sin\left(\frac{\Delta m^2_{ij}L}{2E}\right). \end{aligned} \tag{I.2}$$

Note that we are only considering vacuum oscillations here. Since we are considering

neutrinos from astrophysical sources the propagation length L is very large. Therefore, we have a limit $x = \Delta m^2_{ij} L/4E \gg 1$. In this limit oscillations are so rapid that oscillation terms in the probability take on their average values, $\sin^2(x) \to \frac{1}{2}$ and $\sin(2x) \to 0$. After simplification, the probabilities in the flux calculations become

$$P_{\alpha\beta} = \langle P_{\alpha\beta}(L/E) \rangle = \delta_{\alpha\beta} - 2 \sum_{i>j} \mathrm{Re}(U^*_{\alpha i} U_{\beta i} U^*_{\beta j} U_{\alpha j}) = \sum_i |U_{\alpha i}|^2 |U_{\beta i}|^2. \qquad \text{(I.3)}$$

Writing out the full expression for the propagation matrix P, we can easily see that it's symmetric ($P_{\alpha\beta} = P_{\beta\alpha}$) with the sum of elements in any row or column equal to unity. Now The degree of freedom in the P matrix is reduced to 3 from 4 (3 mixing angles and 1 CP phase), thanks to the quantum ensemble average.

In spite of significant experimental progress there are still many alternative routes in constructing models of neutrino masses and mixing. This variety is mostly due to the considerable ambiguities that remain. First of all, the LSND signal implicates the existence of at least four neutrinos. Then, as neutrino oscillations only determine mass squared differences, a crucial missing point is the absolute scale of neutrino masses. Also the pattern of the neutrino mass spectrum is unknown; it could be approximately degenerate with $m^2 \gg \Delta m^2_{ij}$, or of the inverse hierarchy type (with the solar doublet on top), or of the normal hierarchy type (with the solar doublet below). As for the three mixing angles, the most popular model used to be the Tri-bimaximal mixing where both θ_{13} and $\theta_{23} - \pi/4$ exactly vanish (or more precisely, they vanish in a suitable limit, with correction terms that can be made negligibly small) and, in addition, $s_{12} \sim 1/\sqrt{3}$, a value which is in very good agreement with present data. Correspondingly, the typical A4 discrete group has been applied to explain the mixing pattern as well as many other models in group theory.

Facing the small but nonzero neutrino mass, the see-saw mechanism has been implemented extensively to accommodate it. This mechanism, proposed at the end of the seventies, is based on Dirac and Majorana mass terms. It is now the most natural and viable

mechanism of neutrino mass generation. In order to explain the main idea of the mechanism, let us consider the simplest case of one family. The three parameters m_L, m_D, and m_R characterize, correspondingly, left-handed Majorana, Dirac and right-handed Majorana mass terms. Particles with definite masses are Majorana particles. The main assumptions of the seesaw mechanism is:

- we assume that there is no left-handed Majorana mass term, i.e. that

$$m_L = 0$$

- we assume that the Dirac mass term is generated by the Standard Higgs mechanism, i.e. that m_D is of the order of a mass of quark or lepton

- the right-handed Majorana mass term breaks conservation of the lepton number, and we assume that the lepton number is violated at a scale which is much larger than the electroweak scale, i.e. that

$$m_R \equiv M_R >> m_D.$$

Recalling the form of the neutrino mass matrix

$$M = \begin{bmatrix} m_L & m_D \\ m_D & m_R \end{bmatrix}, \tag{I.4}$$

it follows that the mass eigenvalues of the Majorana particles are given by the expressions

$$m_1 \simeq \frac{m_D^2}{M_R} \ll m_D, \;\; m_2 \simeq M_R \gg m_D. \tag{I.5}$$

In the framework of the seesaw mechanism, smallness of neutrino masses with respect to masses of quarks and leptons is connected with violation of the total lepton number at a large scale given by M_R. The suppression factor $(\frac{m_D}{M_R})$ is characterized by the ratio of

the electroweak scale and the scale of the violation of the lepton number. Note that if we put $m_D \simeq m_t \simeq 170$ GeV and $m_1 \simeq 5 \cdot 10^{-2}$eV (the mass of the heaviest neutrino of the three known neutrinos) we find that $M_R \simeq \frac{m_D^2}{m_1} \simeq 10^{15}$ GeV. Values of neutrino masses and neutrino mixing angles are determined by the concrete form of matrices m_D and M_R. The appearance of large M_R in denominator guarantees the smallness of neutrino masses with respect to masses of leptons and quarks. Thus, if the seesaw mechanism is realized in nature, then:

- Neutrinos are Majorana particles.
- Neutrino masses are much smaller than lepton and quark masses.
- Heavy Majorana particles, the seesaw partners of neutrinos, must exist.

In summary, we have considered all possible neutrino mass terms in the case of three flavor neutrino fields ν_{eL}, $\nu_{\mu L}$, $\nu_{\tau L}$ and three sterile fields ν_{eR}, $\nu_{\mu R}$, $\nu_{\tau R}$. Neutrinos are the Majorana particles if the mass term is not invariant under the global gauge transformations and, therefore, there are no conserved lepton numbers. Neutrinos are Dirac particles if the total lepton number $L = L_e + L_\mu + L_\tau$ is conserved. As neutrino mass matrix is non-diagonal, the fields of the flavor neutrinos ν_{lL} are mixtures of the left-handed components of the fields of neutrinos with definite masses. We use the PMNS matrix to quantize this transformation. The minimal number of the massive neutrinos is equal to the number of the flavor neutrinos (three). If more than three neutrino masses are small, sterile neutrinos must exist. In that case, left-handed flavor neutrinos ν_e, ν_μ and ν_τ will transfer into the sterile neutrinos which have not to date been produced in weak processes or detected via the standard weak interaction.

I.4 Cosmic Neutrino Pevatrons: A Brand New Pathway to Astronomy, Astrophysics, and Particle Physics

Neutrinos serve as unique astronomical messengers. The announcement by the IceCube Collaboration of the observation of cosmic neutrino candidates has signified the beginning of neutrino astroparticle physics. We are facing the obvious question: "Where in the Cosmos are these neutrinos coming from?" There are many possibilities, including origins at either Galactic or extragalactic celestial objects. Except for oscillations, neutrinos propagate without interactions between source and Earth (ignoring their own small magnetic moment), bringing powerful probes of high energy astroparticle physics. The neutrino's direction and energy are preserved, and the neutrino's flavor is altered in a calculable way. In particular, the flavor composition of neutrinos originating at astrophysical sources can serve as a probe of new physics in the electroweak sector. Neutrino (antineutrino) interactions with matter can be reduced to two categories: charged current (CC) interactions in which the neutrino becomes a charged lepton and neutral current (NC) interactions in which the internal state neutrino produces a neutrino rather than a lepton in the final state. The nucleon-neutrino cross section rises roughly linearly with incident energy. For neutrino telescopes located on Earth (e.g. IceCube), the detection (survival) probability is modulated by a combination of the neutrino energy E_ν and the arrival zenith angle θ.

As for the IceCube detector, event topologies are classified as cascades, tracks, or combinations of these. We will discuss in more detail the various event topologies. In short, cascades are generated by ν_e or ν_τ CC interactions and all NC interactions while tracks are generated by ν_μ CC interactions.

A nearly guaranteed neutrino flux originates from interactions of ultra-high energy cosmic rays en route to Earth. Ultrahigh energy protons above the $p\gamma$ production threshold interact with the cosmic microwave and infrared backgrounds as they propagate over cosmological distances [2]. These interactions generate pions, which decay to produce neutrinos. By designing an experiment to find these cosmological neutrinos, the two (now

three) highest energy neutrinos ever observed were recently uncovered [3]. We will conduct a systematic study on the possible origins of these events by focusing the variation of the propagation matrix as well as the signal for $\bar{\nu}_e$ at the Glashow resonance (defined in Chapter IV). Note that events at the Glashow resonance provide the only known physics calibration of neutrino detectors in this high energy range.

For illustration, the main properties of these events observed between May 2010 to May 2012 are given in Table I.1. The arrival directions of the 28 neutrinos are shown in Fig. I.2. We can partition the observation into three bins:

- 26 events from 50 TeV to 1 PeV, which includes the $\sim$ 10 atmospheric background events;
- 2 events from 1 PeV to 2 PeV;
- zero events above 2 PeV.

Naively summarizing, there are three main concerns with the current data:

- there is a gap of events between 400 TeV and 1 PeV;
- the lack of track events does not agree with the popular injection model;
- no observation of Glashow Resonance events suggest either a high energy cutoff or negligible $\bar{\nu}_e$ ratio in the cosmic source.

As more data become available in the near future, it would be possible to tackle these problems. This dissertation consists of my four papers [4; 5; 6; 7] between 2012 and 2015. Therefore, the data we used in this work is up to late 2015, but the analyses are still valid.

ID	Dep. Energy (TeV)	Time (MJD)	Decl. (deg.)	R.A. (deg.)	Med. Angular Error (deg.)	Event Type
1	$47.6^{+6.5}_{-5.4}$	55351.3222110	-1.8	35.2	16.3	Shower
2	117^{+15}_{-15}	55351.4659612	-28.0	282.6	25.4	Shower
3	$78.7^{+10.8}_{-8.7}$	55451.0707415	-31.2	127.9	$\lesssim 1.4$	Track
4	165^{+20}_{-15}	55477.3930911	-51.2	169.5	7.1	Shower
5	$71.4^{+9.0}_{-9.0}$	55512.5516214	-0.4	110.6	$\lesssim 1.2$	Track
6	$28.4^{+2.7}_{-2.5}$	55567.6388084	-27.2	133.9	9.8	Shower
7	$34.3^{+3.5}_{-4.3}$	55571.2585307	-45.1	15.6	24.1	Shower
8	$32.6^{+10.3}_{-11.1}$	55608.8201277	-21.2	182.4	$\lesssim 1.3$	Track
9	$63.2^{+7.1}_{-8.0}$	55685.6629638	33.6	151.3	16.5	Shower
10	$97.2^{+10.4}_{-12.4}$	55695.2730442	-29.4	5.0	8.1	Shower
11	$88.4^{+12.5}_{-10.7}$	55714.5909268	-8.9	155.3	16.7	Shower
12	104^{+13}_{-13}	55739.4411227	-52.8	296.1	9.8	Shower
13	253^{+26}_{-22}	55756.1129755	40.3	67.9	$\lesssim 1.2$	Track
14	1041^{+132}_{-144}	55782.5161816	-27.9	265.6	13.2	Shower
15	$57.5^{+8.3}_{-7.8}$	55783.1854172	-49.7	287.3	19.7	Shower
16	$30.6^{+3.6}_{-3.5}$	55798.6271191	-22.6	192.1	19.4	Shower
17	200^{+27}_{-27}	55800.3755444	14.5	247.4	11.6	Shower
18	$31.5^{+4.6}_{-3.3}$	55923.5318175	-24.8	345.6	$\lesssim 1.3$	Track
19	$71.5^{+7.0}_{-7.2}$	55925.7958570	-59.7	76.9	9.7	Shower
20	1141^{+143}_{-133}	55929.3986232	-67.2	38.3	10.7	Shower
21	$30.2^{+3.5}_{-3.3}$	55936.5416440	-24.0	9.0	20.9	Shower
22	220^{+21}_{-24}	55941.9757760	-22.1	293.7	12.1	Shower
23	$82.2^{+8.6}_{-8.4}$	55949.5693177	-13.2	208.7	$\lesssim 1.9$	Track
24	$30.5^{+3.2}_{-2.6}$	55950.8474887	-15.1	282.2	15.5	Shower
25	$33.5^{+4.9}_{-5.0}$	55966.7422457	-14.5	286.0	46.3	Shower
26	210^{+29}_{-26}	55979.2551738	22.7	143.4	11.8	Shower
27	$60.2^{+5.6}_{-5.6}$	56008.6845606	-12.6	121.7	6.6	Shower
28	$46.1^{+5.7}_{-4.4}$	56048.5704171	-71.5	164.8	$\lesssim 1.3$	Track

Table I.1: Properties of the 28 events observed in 2 years. Shown are the deposited electromagnetic-equivalent energy (the energy deposited by the events in IceCube assuming all light was made in electromagnetic showers) as well as the arrival time and direction of each event and its topology (track or shower-like). The events are ordered according to the Modified Julian Date (MJD).

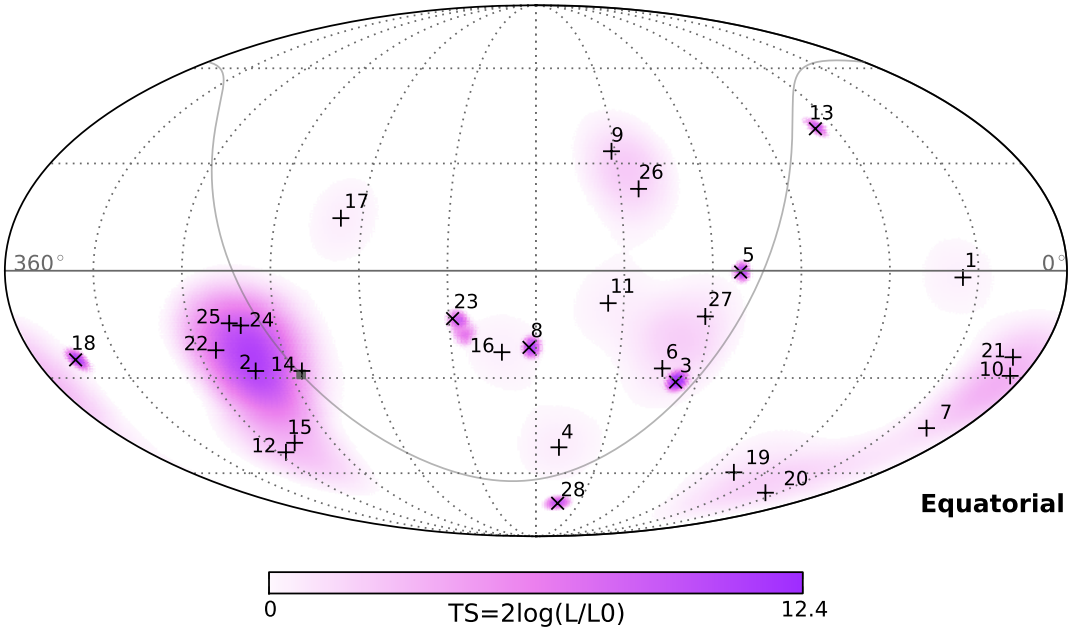

Figure I.2: IceCube skymap in equatorial coordinates of the Test Statistic value (TS) from the maximum likelihood point-source analysis. The most significant cluster consists of five events—all showers and including the second-highest energy event in the sample—with a final significance of 8%. This is not sufficient to identify any neutrino sources from the clustering study. The galactic plane is shown as a gray line with the galactic center denoted as a filled gray square. Best-fit locations of individual events (listed in Table I.1) are indicated with vertical crosses (+) for showers and angled crosses (×) for muon tracks.

CHAPTER II

Cosmic Neutrino Flavor Ratios with Broken ν_μ-ν_τ Symmetry

II.1 Introduction

It is well-known that a statistical average over a neutrino ensemble from cosmic distances eliminates the quantum-mechanical phase $\phi_{jk} \equiv L(m_j^2 - m_k^2)/2E$ between states, leaving a relatively simple result for neutrino-flavor evolution. The evolution $\nu_\alpha \to \nu_\beta$, with α and β any elements of the three-flavor set $\{e,\ \mu,\ \tau\}$, is described by the propagation matrix P whose positive definite elements are

$$P_{\alpha\beta} = \sum_j |U_{\alpha j}|^2 \, |U_{\beta j}|^2 \,. \tag{II.1}$$

The physics behind this formula is that the correct basis for particle propagation is the mass basis, because the particle propagator in field theory is an analytic function with poles at mass values; we sum over the unobserved mass states labeled by j, and we weight each such mass state by its classical probability $|U_{\alpha j}|^2$ to overlap with the flavor α produced at the source, times its classical probability $|U_{\beta j}|^2$ to overlap with the flavor β detected at Earth. The sum on $j = 1, 2, 3$ is over the three active neutrino states. (Astrophysical distances are so much larger than relevant oscillation lengths that subtleties in the definition of cosmic distance [8] are not important here.)

Phase-averaging restores CP-invariance, and so the matrix P describes both neutrino and anti-neutrino propagation. Furthermore, CP-invariance, according to the CPT-theorem, implies also T-invariance, and so the matrix P is symmetric, $P_{\alpha\beta} = P_{\beta\alpha}$. Explicitly, one

has

$$P = \begin{pmatrix} \sum_j |U_{ej}|^2 |U_{ej}|^2 & \sum_j |U_{ej}|^2 |U_{\mu j}|^2 & \sum_j |U_{ej}|^2 |U_{\tau j}|^2 \\ \cdots & \sum_j |U_{\mu j}|^2 |U_{\mu j}|^2 & \sum_j |U_{\mu j}|^2 |U_{\tau j}|^2 \\ \cdots & \cdots & \sum_j |U_{\tau j}|^2 |U_{\tau j}|^2 \end{pmatrix} \tag{II.2}$$

Thus, the flavor ratio unit-vector injected at the source, $\vec{W} \equiv (W_e, W_\mu, W_\tau)$ is measured at Earth to be $\vec{w} \equiv (w_e, w_\mu, w_\tau)$, where

$$\vec{w} = P\vec{W}\,. \tag{II.3}$$

If P is an invertible matrix (i.e., has a nonvanishing determinant), then the inverse equation

$$\vec{W} = P^{-1}\vec{w} \tag{II.4}$$

allows one to input the neutrino flavor ratios observed at Earth to obtain the flavor ratios dynamically injected at the cosmic source. At present, the only observed sources of extra-terrestrial neutrinos are from the Sun and SN1987A. The hope is that neutrino telescopes, recently deployed [9; 10], or soon to be deployed [11], will begin to observe neutrinos from more distant sources. When an ensemble of neutrino events are collected, track-topologies will allow one to glean the ratios of flavors arriving at Earth [12]. Very recently, the IceCube experiment has announced what is likely the first observation of high-energy extra-galactic neutrinos, two showering events characteristic of ν_e's (or $\bar{\nu}_e$'s, since the experiments cannot distinguish ν from $\bar{\nu}$), with energies $\sim$PeV. It appears that the era of neutrino astrophysics is suddenly upon us.

On the terrestrial neutrino experimental front, neutrino mixing data were consistent with ν_μ-ν_τ symmetry, defined operationally as $|U_{\mu j}| = |U_{\tau j}|$, until very recently. The popular example of such a ν_μ-ν_τ symmetric model is the TriBimaximal (TBM) model [13], which

has the following classical probability and flavor propagation matrices:

$$|U_{\alpha j}|^2 = \frac{1}{6}\begin{pmatrix} 4 & 2 & 0 \\ 1 & 2 & 3 \\ 1 & 2 & 3 \end{pmatrix} = \begin{pmatrix} 0.667 & 0.333 & 0 \\ 0.167 & 0.333 & 0.500 \\ 0.167 & 0.333 & 0.500 \end{pmatrix}, \tag{II.5}$$

and

$$P_{\text{TBM}} = \frac{1}{18}\begin{pmatrix} 10 & 4 & 4 \\ 4 & 7 & 7 \\ 4 & 7 & 7 \end{pmatrix} = \begin{pmatrix} 0.55 & 0.22 & 0.22 \\ 0.22 & 0.39 & 0.39 \\ 0.22 & 0.39 & 0.39 \end{pmatrix}. \tag{II.6}$$

With exact ν_μ-ν_τ symmetry, the second and third rows of the $|U|^2$ matrix and the second and third columns of the P matricx are identical, by definition. Accordingly, the determinant of matrix P vanishes, and the matrix is not invertible. Thus, prior theoretical work, which attempted to relate flavor ratios at Earth to the ratios injected at the cosmic sources, guessed at the source ratios and and evolved the guesses forward with Eq. (III.1) to obtain the observable ratios at Earthly detectors. Popular guesses are the pion decay-chain flavor-ratios $\frac{1}{3}$(1:2:0), the β-beam ratios (1:0:0) [14], and the incomplete pion decay-chain or quenched μ-decay ratios (0:1:0) [15]. We will examine flavor evolution in these three injection models in some detail below. A thoughtful overview of neutrino injection models is given in [16].

More satisfying would be to approach the study with observed flavor ratios, and evolve them backwards via Eq. (V.6) to obtain as directly as possible the astrophysical quantities of interest, namely the flavor ratios injected at the sources. Recent neutrino data from nuclear reactors reveals that the ν_μ-ν_τ symmetry is broken. Hence, the determinant of P is no longer vanishing, and the inverse flavor propagation matrix P^{-1} is calculable.

The first purpose of this work is to provide this inverse propagation matrix. As the second purpose of this investigation, we will draw various phenomenological inferences for three-flavor neutrino astrophysics. For example, we will plot the movement of Earthly fla-

vor ratios away from their TriBiMaximal values, for the three most popular cosmic-source flavor models; present a relation among flavor ratios at Earth that determines whether tau neutrino's are injected at the source; derive a general formula for the injection flavor ratio at the source in terms of the observable ratio of readily measurable track and shower events at Earth; and derive bounds on the possible flavor ratios to be observed on Earth, as implied by the measured mixing angles. If observations at Earth were to violate these latter bounds, then some physics other than flavor mixing via phase-averaged vacuum oscillations would be at play. Examples of new physics could be neutrino decay [17], oscillations into new states such as sterile neutrinos or pseudo-Dirac states [18], or new long-range flavor changing neutrino interactions [19].

II.2 Two-Component Flavor – The TBM Example

It is instructive to see how flavor bounds may be derived in the simple case of TBM mixing. The ν_μ-ν_τ symmetry tells us that ν_μ and ν_τ will arrive in equal numbers, regardless of the flavor distribution at the source. Thus, there are but two relevant flavor ratios at Earth, w_e and $w_{\not e}$, with $w_{\not e}$ equally split between ν_μ and ν_τ, and $w_e + w_{\not e} = 1$. We may obtain the propagation matrix in this $(e, \not e)$ basis by adding the identical ν_μ and ν_τ rows in Eq. (II.6), and omitting the now redundant third column. One gets

$$P^{\rm eff}_{\rm TBM} = \frac{1}{9}\begin{pmatrix} 5 & 2 \\ 4 & 7 \end{pmatrix}. \tag{II.7}$$

The propagation equation

$$\begin{pmatrix} w_e \\ w_{\not e} \end{pmatrix} = P^{\rm eff}_{\rm TBM}\begin{pmatrix} W_e \\ W_{\not e} \end{pmatrix} \tag{II.8}$$

is linear, so the flavor extremes at Earth are found by inputting into Eq. (II.8) the pure flavor vectors $\vec{W} = (1,0)$ and $\vec{W} = (0,1)$ at the source. The results are trivially $2/9 \leq w_e \leq 5/9$, correlated with $7/9 \geq w_{\not e} \geq 4/9$. Such is the allowed region of flavor space at Earth ($\vec{w}$) in

the TBM model.

Proceeding further, the determinant of $P^{\rm eff}_{\rm TBM}$ is nonzero, and so this matrix is invertible. The inverse matrix is

$$(P^{\rm eff}_{\rm TBM})^{-1} = \frac{1}{3}\begin{pmatrix} 7 & -2 \\ -4 & 5 \end{pmatrix}, \begin{pmatrix} W_e \\ W_{\not e} \end{pmatrix} = (P^{\rm eff}_{\rm TBM})^{-1} \begin{pmatrix} w_e \\ w_{\not e} \end{pmatrix}. \tag{II.9}$$

From Eq. (II.9) we derive an interesting expression relating flavor ratios at the source to the same ratio observed at Earth:

$$\frac{W_e}{W_{\not e}} = \frac{7\left(\frac{w_e}{w_{\not e}}\right) - 2}{5 - 4\left(\frac{w_e}{w_{\not e}}\right)}. \tag{II.10}$$

Neutrino telescopes are particularly adept at distinguishing muon tracks due to ν_μ interactions, from showering events due to ν_e and ν_τ interactions (neutral current interactions deposit much less energy from the hadronic vertex and may be ignorable in a falling energy spectrum). We may bin together the latter events as $w_{sh} \equiv w_e + w_\tau$. Then, inputting the TBM relations $w_e = w_{sh} - w_\mu$ and $w_{\not e} = 2w_\mu$ into Eq. (II.10), we get an alternative expression of the same relation,

$$\frac{W_e}{W_{\not e}} = \frac{7 - 11\left(\frac{w_\mu}{w_{sh}}\right)}{14\left(\frac{w_\mu}{w_{sh}}\right) - 4}. \tag{II.11}$$

These TBM relations, Eqs.(II.10) and (II.11), hold for any injection model. If either LHS were output, its value would discriminate among injection models.

Theory strongly suggests that ν_τ production at the source is very small [20; 21] (i.e., W_τ is zero or nearly so, or equivalently, that $W_{\not e} \approx W_\mu$). In hand with this assumption, the inverse matrix $(P^{\rm eff}_{\rm TBM})^{-1}$ of Eq. (II.9) provides a complete reconstruction of the flavor ratios at the source in terms of flavor ratios observed at Earth, for the TBM-mixing model.

II.3 Broken ν_μ-ν_τ Symmetry and Three-Component Flavor

With the observation of θ_{13} far from zero, we learn that ν_μ-ν_τ symmetry is likely broken, and an analysis of the full three-component vectors $\vec{w}$ and $\vec{W}$ of Eqs. (III.1) and (V.6) is warranted. Let us begin with a short review of the evidence for broken ν_μ-ν_τ symmetry.

Following [22], the three-neutrino mixing matrix is conventionally parameterized by three planar rotations, analogous to the three Euler angles of classical mechanics, and a purely quantum-mechanical Dirac phase δ [1]:

$$U_{PMNS} \equiv R_{32}(\theta_{32})\, R_{13}(\theta_{13},\delta)\, R_{12}(\theta_{12})\,. \tag{II.12}$$

The double argument of R_{13} is a reminder that by convention, the quantum mechanical Dirac phase appears in the off-diagonal elements of the rotation in the 13-plane:

$$R_{13} = \begin{pmatrix} \cos\theta_{13} & \sin\theta_{13} e^{-i\delta} \\ -\sin\theta_{13} e^{+i\delta} & \cos\theta_{13} \end{pmatrix}. \tag{II.13}$$

The range for the angles is $[0,\pi/2]$, while the range for the phase is $[-\pi,+\pi]$, or equivalently, $\cos\delta \in [-1,+1]$.

In terms of the three angles and the single phase, one finds that the conditions $|U_{\mu j}| = |U_{\tau j}|$ for ν_μ-ν_τ symmetry require that (i) $\theta_{32} = \pi/4$ and (ii) $\sin(2\theta_{12})\sin\theta_{13}\cos\delta = 0$.

Choices of angles/phase which satisfy (ii) above, necessary to uphold the ν_μ-ν_τ symmetry, are [23]:

- Case (a): $\theta_{13} = 0$ (TBM mixing is a special subcase of $\theta_{13} = 0$, wherein $\sin\theta_{12}$ is set to $1/\sqrt{3}$);
- Case (b): $\theta_{12} = 0$ or $\pi/2$;

[1] The simplest relations between the three angles and three mixing moduli are $|U_{e3}|^2 = s^2_{13}$, $|U_{e2}|^2 = c^2_{13}s^2_{12}$, and $|U_{\mu 3}|^2 = c^2_{13}s^2_{32}$. Also simple are $|U_{e1}|^2 = c^2_{13}c^2_{12}$ and $|U_{\tau 3}|^2 = c^2_{13}c^2_{32}$, but these two are not independent of the other three relations. There is a fourth independent $|U_{\alpha j}|^2$, which must be chosen from the set $\{|U_{\mu 1}|^2, |U_{\mu 2}|^2, |U_{\tau 1}|^2, |U_{\tau 2}|^2\}$. The independence of four $|U_{\alpha j}|^2$'s corresponds to the independent three mixing angles plus one Dirac phase δ.

- Case (c): $\cos\delta = 0$, i.e. $\delta = \pm\pi/2$.

The recent spectacular evidence that $\theta_{13} \sim 9^\circ$ is not only nonzero, but many σ from zero, rules out case (a). The value of θ_{12} is inferred from experiment to be far from either zero or $\pi/2$, which rules out case (b). (In addition, the matter effect responsible for suppression of ν_e from the sun requires $|U_{e1}| > |U_{e2}| > 0$, which also rules out case (b).)

Finally, we are left to discuss case (c). There is little experimental constraint on δ, for it occurs (Eq. (II.13)) with $\sin\theta_{13}$ as a prefactor. Recent experimental evidence suggests that θ_{32} is not equal to the maximal-mixing value $\pi/4$. Case (c) is mildly disfavored by data. So it appears that ν_μ-ν_τ symmetry is likely broken. If so, then P is an invertible matrix. And even if θ_{32} were exactly equal $\pi/4$, it still remains a possibilty that ν_μ-ν_τ symmetry is broken by a value $\delta \neq \pm\pi/2$. In the rest of this section we proceed to analyze 3-neutrino flavor propagation in the now favored case of a (slightly) broken ν_μ-ν_τ symmetry.

II.3.1 Three-Flavor Analysis

The constraint $W_e + W_\mu + W_\tau = 1$ reduces the three-dimensional W_e, W_μ, W_τ-space to the physical triangle with corners at $(1,0,0)$, $(0,1,0)$, and $(0,0,1)$. Because the relation in Eq. (III.1) is linear in $\vec{W}$, the extremes of $\vec{w}$ are obtained from the values of $\vec{W}$ at these corners. The result is

$$\max / \min\{w_\alpha\} = \max / \min\{P_{\alpha e}, P_{\alpha\mu}, P_{\alpha\tau}\}\,. \tag{II.14}$$

(The two-component analog of this result was presented below Eq. (II.8).)

For the theoretical expectation that ν_τ's are not produced by the cosmic mechanisms, $W_\tau = 0$ and the extremes of $\vec{w}$ are even simpler:

$$\max / \min\{w_\alpha\} = \max / \min\{P_{\alpha e}, P_{\alpha\mu}\}\,,\ (\text{no source } \nu_\tau\text{'s}) \tag{II.15}$$

These simply-stated results have profound meaning. For example, a measurement of any

w_α satisfying Eq. (II.14) but not satisfying (II.15) would establish that in fact ν_τ's are produced at cosmically-distant sources. (Note that there is no two-component analog of the $W_\tau = 0$ result, because with the parameter $W_{\not e}$ does not distinguish among W_τ and W_μ.)

Inversion of the symmetric 3×3 matrix P yields the symmetric inverse matrix

$$P^{-1} = \frac{1}{\mathrm{Det}(P)} \begin{pmatrix} (P_{\mu\mu}P_{\tau\tau} - P_{\mu\tau}^2) & (P_{e\tau}P_{\mu\tau} - P_{e\mu}P_{\tau\tau}) & (P_{e\mu}P_{\mu\tau} - P_{e\tau}P_{\mu\mu}) \\ \cdots & (P_{ee}P_{\tau\tau} - P_{e\tau}^2) & (P_{e\tau}P_{e\mu} - P_{ee}P_{\mu\tau}) \\ \cdots & \cdots & (P_{ee}P_{\mu\mu} - P_{e\mu}^2) \end{pmatrix} . \quad \text{(II.16)}$$

With this P^{-1} matrix in hand, we may directly calculate the injection ratios $\vec{W} = P^{-1}\vec{w}$ once the Earthly ratios $\vec{w}$ are measured. This matrix, along with the numerical values given below for its matrix elements, are among our main results.

As mentioned earlier, the inverse of P does not exist for the TBM model, because $\mathrm{Det}(P_{\mathrm{TBM}})$ vanishes. However, the sign-weighted cofactor matrix ($(-1)^{\alpha+\beta}$ timing the cofactor of $(P_{\mathrm{TBM}})_{\alpha\beta}$) does exist, and its form sheds light on what one can expect in the realistic three-neutrino case for the relative values of matrix elements in P^{-1}. From the values of the TBM matrix in Eq. (II.6), one can easily calculate the sign-weighted cofactor matrix, "$\mathrm{Det}(P)\,P^{-1}$", even for matrices with a vanishing determinant. (The quotation marks here are merely a reminder that "$\mathrm{Det}(P)\,P^{-1}$" is just a convenient label for the sign-weighted cofactor matrix.) We get

$$\text{“}[\mathrm{Det}(P_{\mathrm{TBM}})\,(P_{\mathrm{TBM}})^{-1}]\text{”} = \frac{1}{6} \begin{pmatrix} 0 & 0 & 0 \\ 0 & 1 & -1 \\ 0 & -1 & 1 \end{pmatrix} , \quad \text{(II.17)}$$

and we repeat for the reader that the right-hand side of this relation is calculated independently of $\mathrm{Det}(P)$. Because the updated values of the mixing angles break the ν_μ-ν_τ

symmetry implicit in the TBM model by only a small amount, we may expect that with updated values of mixing angles, matrix element values similar to those of Eq. (II.17) will result for "$\mathrm{Det}(P)\,P^{-1}$", and a texture similar to that in Eq. (II.17) will result for the inverse matrix P^{-1}.

Of course, with small ν_μ-ν_τ symmetry breaking, $\mathrm{Det}(P)$ will also be small, but as long as it is nonzero, the matrix P is invertible.

It is instructive to see how the shift in $\mathrm{Det}(P)$ will happen. $\mathrm{Det}(P)$ is unchanged when we subtract the second row of P from the bottom row, and then subtract the second column of P from the third column. After a bit of algebra, the result is

$$\mathrm{Det}(P) = \begin{vmatrix} P_{ee} & P_{e\mu} & \sum_j |U_{ej}|^2 \Delta_j \\ P_{e\mu} & P_{\mu\mu} & \sum_j |U_{\mu j}|^2 \Delta_j \\ \sum_j |U_{ej}|^2 \Delta_j & \sum_j |U_{\mu j}|^2 \Delta_j & \sum_j \Delta_j \Delta_j \end{vmatrix} \tag{II.18}$$

where $\Delta_j \equiv |U_{\tau j}|^2 - |U_{\mu j}|^2$ are the three parameters characterizing the breaking of ν_μ-ν_τ symmetry [24]. Only two of the three Δ_j are independent, since $\sum_j \Delta_j = \sum_j |U_{\mu j}|^2 - \sum_j |U_{\tau j}|^2 = 1 - 1 = 0$. The symmetry of P allows the row subtraction and column subtraction in $\mathrm{Det}(P)$ to each introduce a factor of Δ_j, leading to a determinant that is of order $(\Delta_j \Delta_k)$, very small. In the form of Eq. (V.7), the determinant is easily evaluated. The result is

$$\begin{aligned} \mathrm{Det}(P) = & \left(\sum_j \Delta_j \Delta_j \right) \left(P_{ee} P_{\mu\mu} - P_{e\mu}^2 \right) \\ & + \sum_{j,k} \Delta_j \Delta_k \left(2 P_{e\mu} |U_{ej}|^2 |U_{\mu k}|^2 - P_{\mu\mu} |U_{ej}|^2 |U_{ek}|^2 - P_{ee} |U_{\mu j}|^2 |U_{\mu k}|^2 \right) . \end{aligned} \tag{II.19}$$

In terms of the mixing angles and Dirac phase, we note that the ν_μ-ν_τ symmetry-breaking

parameters have expressions

$$\begin{aligned}
\Delta_1 &= c(2\theta_{32})\,(c_{12}^2 s_{13}^2 - s_{12}^2) - s(2\theta_{12})\,s(2\theta_{32})\,s_{13}\cos\delta\,, \\
\Delta_2 &= c(2\theta_{32})\,(s_{12}^2 s_{13}^2 - c_{12}^2) + s(2\theta_{12})\,s(2\theta_{32})\,s_{13}\cos\delta\,, \\
\Delta_3 &= c(2\theta_{32})\,c_{13}^2\,. \qquad \text{(II.20)}
\end{aligned}$$

II.3.2 Three-Flavor Numerics

Perturbative expansions about TBM values for neutrino flavor ratios and for the inference of the Dirac phase δ have been considered previously, both before [25] the measurement of θ_{13}, and after [26]. None of the prior work considers the inversion of the propagation matrix. In what follows, we will not appeal to a perturbative expansion; rather, we will use central values and errors from the most recent direct fits of the PMNS matrix parameters to global data. Using the notation $[-2\sigma, \text{best fit}, +2\sigma]$, we summarize the global analysis of [27] as

$$\begin{aligned}
\sin^2\theta_{13} &\subset [0.019,\quad \mathbf{0.0246},\quad 0.030]\,, \\
\sin^2\theta_{32} &\subset [0.38,\ \mathbf{0.613}/\mathbf{0.427}, 0.66]\,, \qquad \text{(II.21)}
\end{aligned}$$

if the neutrino mass-squared ordering displays a "normal" hierarchy (i.e., $(m_3^2 - m_2^2) \gg (m_2^2 - m_1^2) > 0$); and slightly different,

$$\begin{aligned}
\sin^2\theta_{13} &\subset [0.020, \mathbf{0.0250}, 0.030]\,, \\
\sin^2\theta_{32} &\subset [0.39,\ \mathbf{0.600},\ 0.65\,]\,, \qquad \text{(II.22)}
\end{aligned}$$

if the hierarchy is "inverted" (i.e., $(m_2^2 - m_3^2) \gg (m_2^2 - m_1^2) > 0$). The mass ordering $m_1 < m_2$ is fixed by the matter effect in the Sun needed to explain the observed solar ratio $w_e \sim 1/3$. This leaves the two possible hierarchical orderings identified above. The claim is made in Ref. [27] that $\sin^2\theta_{13}$ is $10.2\,\sigma$ away from zero. The first and second "best fit" options

for $\sin^2\theta_{32}$ in the normal hierarchy reflect an octant ambiguity in the present data. We remark that $\sin^2\theta_{32}$ is not maximal in the best fit value, nor within the 1σ error, but may be maximal at 2σ.

For either hierarchy, the remaining results of the global fit concern $\sin^2\theta_{12}$ and $\cos\delta$:

$$\sin^2\theta_{12} \subset [\, 0.29, \mathbf{0.320}, 0.35\,], \tag{II.23}$$

which shows that $\sin^2\theta_{12}$ is many σ away from either zero or the maximal value of $1/2$. For $\cos\delta$, at even 1σ the entire range of $[-1,+1]$ is allowed. We remark that even though our propagation matrix elements $P_{\alpha\beta}$ have a classical explanation (given in the introduction), they nevertheless depend on the quantum mechanical "Dirac phase" parameter δ, via the *CP*-conserving factor $\mathrm{Re}(e^{i\delta}) = \cos\delta$. We will take three typical values $(0,+1,-1)$ for the unconstrained parameter $\cos\delta$. The global analyses of [28; 29] find numbers similar to those used here [27]. We note that for the choice $\cos\delta = 0$, the deviation of θ_{32} from maximality ($\pi/4$) is the sole source of ν_μ-ν_τ symmetry breaking. (Accordingly, $\mathrm{Det}(P)$ will be very small for the choice $\cos\delta = 0$.)

Experiments necessarily determine the above parameters in combinations. Accordingly, the parameter errors quoted above are correlated. We will take these errors as uncorrelated, since the alternative requires an independent global fit for each change of any parameter [30]. Treating the errors as uncorrelated is conservative in that it allows a larger range of parameter values for a given confidence level.

We illustrate the result of the global best fit for the normal hierarchy case, with $\theta_{32} < \pi/4$. The three entries per matrix correspond to three assumed values for the Dirac CP

phase, with ordering $\cos\delta = 0, +1, -1$. We find:

$$|U_{\alpha j}|^2 = \begin{pmatrix} 0.663 & 0.312 & 0.0246 \\ 0.191 & 0.393 & 0.416 \\ 0.146 & 0.295 & 0.559 \end{pmatrix}, \begin{pmatrix} 0.663 & 0.312 & 0.0246 \\ 0.263 & 0.321 & 0.416 \\ 0.0738 & 0.368 & 0.559 \end{pmatrix}, \begin{pmatrix} 0.663 & 0.312 & 0.0246 \\ 0.118 & 0.465 & 0.416 \\ 0.219 & 0.222 & 0.559 \end{pmatrix}; \tag{II.24}$$

and the symmetric matrices

$$P = \begin{pmatrix} 0.538 & 0.259 & 0.203 \\ \cdots & 0.364 & 0.377 \\ \cdots & \cdots & 0.421 \end{pmatrix}, \begin{pmatrix} 0.538 & 0.285 & 0.177 \\ \cdots & 0.345 & 0.370 \\ \cdots & \cdots & 0.453 \end{pmatrix}, \begin{pmatrix} 0.538 & 0.234 & 0.228 \\ \cdots & 0.404 & 0.362 \\ \cdots & \cdots & 0.410 \end{pmatrix}; \tag{II.25}$$

$$\mathrm{Det}(P)\,P^{-1} = \begin{pmatrix} 0.0115 & -0.0327 & 0.0238 \\ \cdots & 0.185 & -0.150 \\ \cdots & \cdots & 0.129 \end{pmatrix}, \begin{pmatrix} 0.0195 & -0.0633 & 0.0441 \\ \cdots & 0.212 & -0.149 \\ \cdots & \cdots & 0.105 \end{pmatrix}, \begin{pmatrix} 0.0344 & -0.0132 & -0.00750 \\ \cdots & 0.168 & -0.141 \\ \cdots & \cdots & 0.163 \end{pmatrix}; \tag{II.26}$$

$$P^{-1} = \begin{pmatrix} 4.59 & -13.1 & 9.52 \\ \cdots & 74.2 & -60.1 \\ \cdots & \cdots & 51.5 \end{pmatrix}, \begin{pmatrix} 66.9 & -217 & 151 \\ \cdots & 728 & -510 \\ \cdots & \cdots & 359 \end{pmatrix}, \begin{pmatrix} 2.51 & -0.961 & -0.548 \\ \cdots & 12.3 & -10.3 \\ \cdots & \cdots & 11.9 \end{pmatrix}; \tag{II.27}$$

$$\text{where } \mathrm{Det}(P) = (2.50, 0.291, 13.7) \times 10^{-3}\,. \tag{II.28}$$

The $|U|^2$ and P matrices may be compared to the corresponding TBM matrices, given earlier in Eqs. (V.2) and (II.6). The determinant of P_{TBM} vanishes, and so there is no P^{-1}_{TBM} to which one may compare. On the other hand, the matrix $\mathrm{Det}(P)\,P^{-1}$ has the form of the analogous TBM matrix, given in Eq. (II.17).

A visual comparison between the TBM and Nature's choices is given in Fig. II.1. The constraint $w_e + w_\mu + w_\tau = 1$ reduces $\vec{w}$-space to a triangle with corners at (1,0,0), (0,1,0), and (0,0,1). We orient the triangle with w_e at the apex. Then, ν_μ-ν_τ symmetry with its $w_\mu = w_\tau$ defines a vertical line through the center of the triangle. The horizontal distance of the point $\vec{w}$ from the center line provides a kind of measure of ν_μ-ν_τ symmetry breaking.

The left triangle plots (lower-case letters) show the entire $\vec{w}$-parameter space, for three different flavor-injection models for normal (NH) and inverted (IH) neutrino mass hierarchies. In descending order, the plots are:

- (a) NH with pion chain injection,
- (b) NH with quenched muon (incomplete pion chain) injection,
- (c) NH with β-beam injection, and
- (d) IH with β-beam injection.

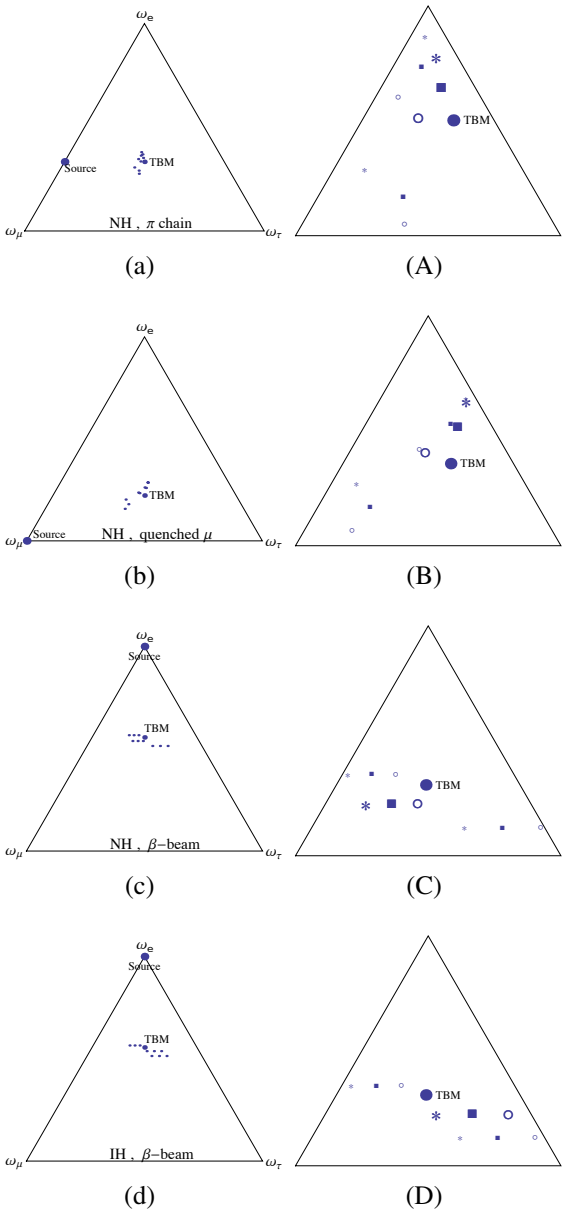

Figure II.1: Triangle plots of (left) entire $\vec{w}$-parameter space, (right) un-normalized blow-up of left panel parameter region. See the main text for an explanation of symbols.

Each plot shows the flavor values for TBM (large solid dot) and nine updated sets of fitted mixing angles: square, star, and open circle correspond to Dirac phase $\delta = \pi/2, 0, \pi$, respectively(i.e. $\cos\delta = (0, 1, -1)$). Larger symbols correspond to best fit values for mixing angles and smaller symbols to $\pm 2\sigma$ values. Combinations of hierarchies and injection models not shown would appear very similar to one of the four plots on display. Right panels (capital letters A,B,C,D) show un-normalized blow-up of left panel parameter region containing the nine predictions and TBM value. ν_μ-ν_τ symmetry predicts a value on the vertical line through the TBM dot; potential deviations from ν_μ-ν_τ symmetry are clear.

II.3.3 Examples of Three-Flavor Phenomenology

Another use of the numerical results is to input the $P_{\alpha\beta}$ values from Eq. (II.25) into Eqs. (II.14) and (II.15). Here we learn, for example, that w_e is bounded, in the NH model with $\theta_{32} < \pi/4$, by a maximum of 0.538, and by a minimum of (0.177, 0.203, 0.228), for $\cos\delta = (0, +1, -1)$. When W_τ is set to zero to conform with theoretical prejudice, then the maximum is not affected but the minimum rises to (0.285, 0.259, 0.234), respectively.

Although the main use of the inverse propagation matrix which we have constructed is implementation of Eq. (V.6) to infer neutrino flavor ratios at the cosmic sources, here we present yet another use for the matrix P^{-1}. Compelling theoretical arguments from particle physics tell us that ν_τ production at the source is very suppressed, due to the heavy τ mass. Thus we expect $W_\tau \sim 0$. This expectation can be easily checked. From Eq. (V.6) we have

$$0 = W_\tau = P^{-1}_{e\tau} w_e + P^{-1}_{\mu\tau} w_\mu + P^{-1}_{\tau\tau} w_\tau \,, \tag{II.29}$$

with the elements of P^{-1} given analytically in Eq. (II.16). Multiplied by $\mathrm{Det}(P)$, this result is

$$\begin{aligned} 0 &= (P_{e\mu}P_{\mu\tau} - P_{e\tau}P_{\mu\mu})\, w_e \\ &+ (P_{e\tau}P_{e\mu} - P_{ee}P_{\mu\tau})\, w_\mu + (P_{ee}P_{\mu\mu} - P^2_{e\mu})\, w_\tau \,, \end{aligned} \tag{II.30}$$

subject to the normalization $w_e + w_\mu + w_\tau = 1$. Numerical values for the parenthetical expressions for the best fit of the normal hierarchy with θ_{32} in the first octant are given in the final columns of Eq. (II.26). Any observed violation of this result would implicate ν_τ production at the sources.

As a final demonstration of the utility of the new, full flavor evolution matrix, we consider the dependence of the flavor ratio W_μ/W_e at the sources on the flavor ratios observed at Earth. Here, we embrace theoretical prejudice and assume that ν_τ's are not produced at the sources, i.e. $W_\tau = 0$. We use Eq. (III.1) to derive the three $w_\alpha(W_e, W_\mu)$, then sum w_e and w_τ to get w_{sh}, from the Earthly ratio $w_\mu(W_e, W_\mu)/w_{sh}(W_e, W_\mu)$, and invert to get

$$\frac{W_\mu}{W_e} = \frac{P_{e\mu} - (P_{ee} + P_{e\tau})\left(\frac{w_\mu}{w_{sh}}\right)}{(P_{e\mu} + P_{\mu\tau})\left(\frac{w_\mu}{w_{sh}}\right) - P_{\mu\mu}}. \tag{II.31}$$

This equation generalizes Eq. (II.11) to the condition of broken ν_μ-ν_τ symmetry. It is independent of any injection model. Therefore, it allows us to infer the flavor ratio of cosmically distant sources from the track-to-shower ratio observed at Earth, and thereby discriminate among injection models. Values for the injection ratio expected from the most popular source models are $\sim (2, \infty, 0)$ for the pion decay-chain, quenched muon, and β-beam models, respectively. These values for the injection ratio are quite different, and so discrimination among popular models via Eq. (II.31) should be straightforward.

II.4 Discussions and Conclusions

Experimental inference of flavor ratios involves some uncertainty. We have neglected these uncertainties in this more theoretical paper. For example, neutrino neutral-current (NC) interactions, the same for all three flavors, contribute to shower events. The ratio of the neutral to charged current cross-sections is known, so the NC contribution can be accounted for in a data sample. As another example, the experimental efficiencies for measuring shower events and muon-track events are different. Again, these can be accounted for in a

data sample.

What we have shown is that neutrino flavor physics is rich in its information content, and therefore worth pursuing. Neutrino flavor physics offers another window into the dynamics of the most distant, most energetic objects in the Universe.

We end with a summary of the main results discussed in this chapter. We have:

- shown the movement of Earthly measured flavor ratios away from the ν_μ-ν_τ symmetric value of the previously viable TriBiMaximal model, for the three most popular cosmic-source flavor models;
- derived the inverse flavor propagation matrix which allows one to infer flavor ratios injected at cosmically-distant sources from the ratios observed here on Earth;
- presented a relation among flavor ratios at Earth that determines whether ν_τ's are injected at the source;
- derived a general formula for the ν_μ/ν_e injection flavor ratio at the source in terms of the observable ratio of track-to-shower events at Earth.

CHAPTER III

Flavor Ratios and Mass Hierarchy at Neutrino Telescopes

III.1 Neutrino Mass Hierarchy

The terrestrial neutrino experiments have been making significant progress towards determining the neutrino properties. For instance, the magnitude of the mass-squared splittings and the mixing angles θ_{12}, θ_{23} have been relatively well measured. For years, the neutrino mixing data have been consistent with $\theta_{13} = 0$. This accommodates the ν_μ-ν_τ symmetry naturally realized by the TriBimaximal (TBM) model [13]. However, DAYA-BAY [31] and RENO [32] have recently observed $\sin^2(2\theta_{13}) = 0.092 \pm 0.016\,(\text{stat.}) \pm 0.005\,(\text{syst.})$ and $\sin^2(2\theta_{13}) = 0.113 \pm 0.013\,(\text{stat.}) \pm 0.019\,(\text{syst.})$ at 68% C.L. respectively. This disfavors the TBM model and represents yet another important step towards the complete understanding of the neutrino sector.

Despite the significant progress made by the experiments, neutrinos remain to be mysterious. We are still ignorant of some basic neutrino properties: Is the neutrino mass hierarchy normal or inverted? Are neutrinos Dirac or Majorana in nature? What is the absolute mass scale of neutrinos? What is the Dirac CP-violating phase? Each of these questions is important on its own. The focus of this chapter is the neutrino mass hierarchy.

Currently, there are a few relatively promising experiments proposed to measure the neutrino mass hierarchy. These include LBNE (accelerator) [33], PINGU (atmospheric) [34] and JUNO (reactor) [35]. The timescale of these experiments ranges from 2025 to 2030 for the first results [36]. The sensitivities of these experiments are quantified in [37; 38; 39].

Up until 2013, the IceCube collaboration has reported an excess of 37 neutrino events relative to the atmospheric neutrino background [3; 40]. Apart from the two events that are almost certainly produced in cosmic-ray air showers, 3 events (among the remaining 35)

have energies slightly above PeV while the other 32 events have energies between 20 TeV and 400 TeV. The overall signal significance is that the analysis rejects a purely atmospheric explanation of these neutrino events at 5.7σ. The hope is that after an ensemble of neutrino events have been collected, track-topologies will allow one to reveal the neutrino flavor ratios arriving on Earth [12].

In this chapter, we study the cosmic neutrino flavor ratios against the Dirac CP-violating phase at neutrino telescopes, taking into account of the charged-current and neutral-current neutrino-nucleon interactions at the detectors. Then, we propose that precise measurements of the cosmic neutrino flavor ratios at neutrino telescopes may provide yet another possible way of determining the neutrino mass hierarchy. As we shall see, the sensitivity of our scheme is independent of the undetermined values of the Dirac CP-violating phase.

III.2 Cosmic Neutrino Flavor Ratios at Neutrino Telescopes

In the standard treatment of neutrino oscillations, neutrino flavor states and mass eigenstates are related by a unitary transformation: $|\nu_\alpha\rangle = \sum_j U^*_{\alpha j} |\nu_j\rangle$, where $\alpha = e, \mu, \tau$ and $j = 1, 2, 3$ are the indices for the flavor states and mass eigenstates respectively. This unitary transformation is described by the PMNS matrix U with the elements $U_{\alpha j} = \langle \nu_\alpha | \nu_j \rangle$.

For a given neutrino flavor ratio unit-vector $\vec{W} \equiv (W_e, W_\mu, W_\tau)$ produced at cosmic sources, the corresponding flavor ratio $\vec{\phi} \equiv (\phi_e, \phi_\mu, \phi_\tau)$ measured on Earth can be obtained from

$$\vec{\phi} = P\vec{W} \,. \tag{III.1}$$

Due to non-zero θ_{13}, the $\nu_\mu - \nu_\tau$ symmetry is broken and P is now invertible. This means that measurements of $\vec{\phi}$ on Earth can now be used to directly reveal $\vec{W}$ through the relation $\vec{W} = P^{-1}\,\vec{\phi}$ [7; 41].

Since τ are not produced at cosmic sources, the initial neutrino flavor compositions generally do not have ν_τ [20; 21; 42; 5]. Although ν_τ may be produced from charmed meson decays, the production of charmed mesons requires a higher energy threshold and it

has a lower cross-section. This means that the amount of ν_τ produced from this channel is negligible [43; 44]. Therefore, it is reasonable to parameterize the most general injection model as $(\,\alpha : 1-\alpha : 0\,)$, where α is a free parameter ranging from 0 to 1.

Neutrino telescopes are particularly adept at distinguishing the muon tracks from the showering events. Thus, an experimentally useful observable would be the track-to-shower ratio:

$$R = \frac{p_{\rm CC}\ \phi_\mu}{p_{\rm NC}\ \phi_\mu + \phi_e + \phi_\tau}\,, \tag{III.2}$$

where $p_{\rm CC}$ and $p_{\rm NC}$ are the probabilities of charged-current (CC) and neutral-current (NC) neutrino-nucleon interactions respectively. Normally, one need to multiply $p_{\rm NC}$ by a factor accounting for the ratio of hadronic energy over neutrino energy. For both ν_μ and $\bar{\nu}_\mu$, the charged-current processes contribute to the track events while the neutral-current processes contribute to the shower events. There will be background events contributing to each of the track and shower events. Hence, R represents the track-to-shower ratio to be observed by neutrino telescopes with the background events subtracted. In general, $p_{\rm CC}$ and $p_{\rm NC}$ are energy-dependent. Around 100 TeV, $p_{\rm CC}$ and $p_{\rm NC}$ stay relatively constant and we have $p_{\rm CC} \approx 0.72$ and $p_{\rm NC} \approx 0.28$ for both ν_μ and $\bar{\nu}_\mu$ (see Tables I and II in [45]). We will take these values for the rest of our study. Notice that for ν_τ and $\bar{\nu}_\tau$ with energies above a few PeV, about 20% of their CC interactions will also contribute to the track events through the "double-bang" events [46], and Eq. (III.2) will need to be modified correspondingly. However, we have explored this modification and found that it does not change the qualitative results in this work. Also, most of the neutrino events observed by IceCube so far have energies below PeV, and so we will just present our results using Eq. (III.2).

For the most general case, we obtain (using $p_{\rm CC} + p_{\rm NC} = 1$)

$$R = \frac{p_{\rm CC}\left[P_{\mu e}\,\alpha + P_{\mu\mu}\,(1-\alpha)\right]}{\left[1-p_{\rm CC}\,P_{\mu e}\right]\,\alpha + \left[1-p_{\rm CC}\,P_{\mu\mu}\right]\,(1-\alpha)}\,. \tag{III.3}$$

Currently, there are three popular models for the production of cosmic neutrinos. They are:

- (1) Pion-Chain: This is by far the most conventional model. Neutrinos could be created from hadronic sources such as $p+p \to \pi^+ \to \mu^+ + \nu_\mu \to e^+ + \nu_e + \nu_\mu + \bar{\nu}_\mu$ or $p+p \to \pi^- \to \mu^- + \bar{\nu}_\mu \to e^- + \bar{\nu}_e + \nu_\mu + \bar{\nu}_\mu$. The high-energy π^+ could also be produced from the interactions between accelerated protons and photons. Both cases lead to $(W_e : W_\mu : W_\tau) = (\frac{1}{3} : \frac{2}{3} : 0)$. This is a special case of Eq. (III.3) with $\alpha = 1/3$:

$$R = \frac{p_{\rm CC}\left(P_{\mu e} + 2P_{\mu\mu}\right)}{\left[1 - p_{\rm CC}P_{\mu e}\right] + 2\left[1 - p_{\rm CC}P_{\mu\mu}\right]}\,. \tag{III.4}$$

  As a remark, in the TBM model [13], we have

$$P_{\rm TBM} = \frac{1}{18}\begin{pmatrix} 10 & 4 & 4 \\ 4 & 7 & 7 \\ 4 & 7 & 7 \end{pmatrix}, \tag{III.5}$$

  which implies that $(\phi_e : \phi_\mu : \phi_\tau)_{\rm TBM} = (\frac{1}{3} : \frac{1}{3} : \frac{1}{3})$. Since the $\nu_\mu - \nu_\tau$ symmetry is slightly broken, we expect the actual $(\phi_e : \phi_\mu : \phi_\tau)$ to deviate slightly from $(\frac{1}{3} : \frac{1}{3} : \frac{1}{3})$.

- (2) Damped-Muon: In the pion decay chain mentioned above, it is possible that the flux of muons gets depleted. This may happen if the muons lose energy in a strong magnetic field or get absorbed in matter [15]. This leads to $(W_e : W_\mu : W_\tau) = (0 : 1 : 0)$ which is a special case of Eq. (III.3) with $\alpha = 0$:

$$R = \frac{p_{\rm CC}\,P_{\mu\mu}}{1 - p_{\rm CC}P_{\mu\mu}}\,. \tag{III.6}$$

- (3) Beta-Beam: Some sources may dominantly emit neutrons. These neutrons could be produced from the photo-dissociation of heavy nuclei [14] or the interactions between accelerated protons and photons [47]. The decays of these neutrons $(n \to p + e^- + \bar{\nu}_e)$ lead to $(W_e : W_\mu : W_\tau) = (1 : 0 : 0)$ which is a special case of Eq.

(III.3) with $\alpha = 1$:

$$R = \frac{p_{\rm CC}\, P_{\mu e}}{1 - p_{\rm CC}\, P_{\mu e}}\,. \tag{III.7}$$

III.3 Flavor Ratios and Mass Hierarchy: Standard Scenario

In this section, we study the standard scenario with three active neutrinos. We first illustrate our idea with the three popular injection models, and then consider the most general injection model.

Throughout the entire discussion, we embrace the most updated global best-fit data of three neutrino mixing [48] for normal hierarchy (NH) and inverted hierarchy (IH):

$$\sin^2\theta_{13} = 0.0234,\ \ \sin^2\theta_{32} = 0.567/0.467,\ \ \sin^2\theta_{12} = 0.323\ \ (\text{NH}), \tag{III.8}$$

$$\sin^2\theta_{13} = 0.0240,\ \ \sin^2\theta_{32} = 0.573,\ \ \sin^2\theta_{12} = 0.323\ \ (\text{IH}). \tag{III.9}$$

Therefore, according to the best-fit analysis in [48], the neutrino mass hierarchy is determined dominantly by θ_{23}. This suggests three possible cases: (1) normal hierarchy with $\sin^2\theta_{32} = 0.567$ (NH1), (2) normal hierarchy with $\sin^2\theta_{32} = 0.467$ (NH2), (3) inverted hierarchy with $\sin^2\theta_{32} = 0.573$ (IH).

Since neutrino telescopes are particularly adept at distinguishing the muon tracks from the showering events, the main observable to be studied in this work is R. The role of the uncertainties of the neutrino mixing parameters in flavor measurements at neutrino telescopes have been discussed before [49; 50]. Now, DAYA-BAY [31] and RENO [32] have already provided us with the precise value for θ_{13}. As far as neutrino oscillation is concerned, the only unknown parameter in the PMNS matrix U is the Dirac CP-violating phase δ [26]. Thus, we will plot R against δ to see the dependence of the sensitivity on the only unknown parameter δ.

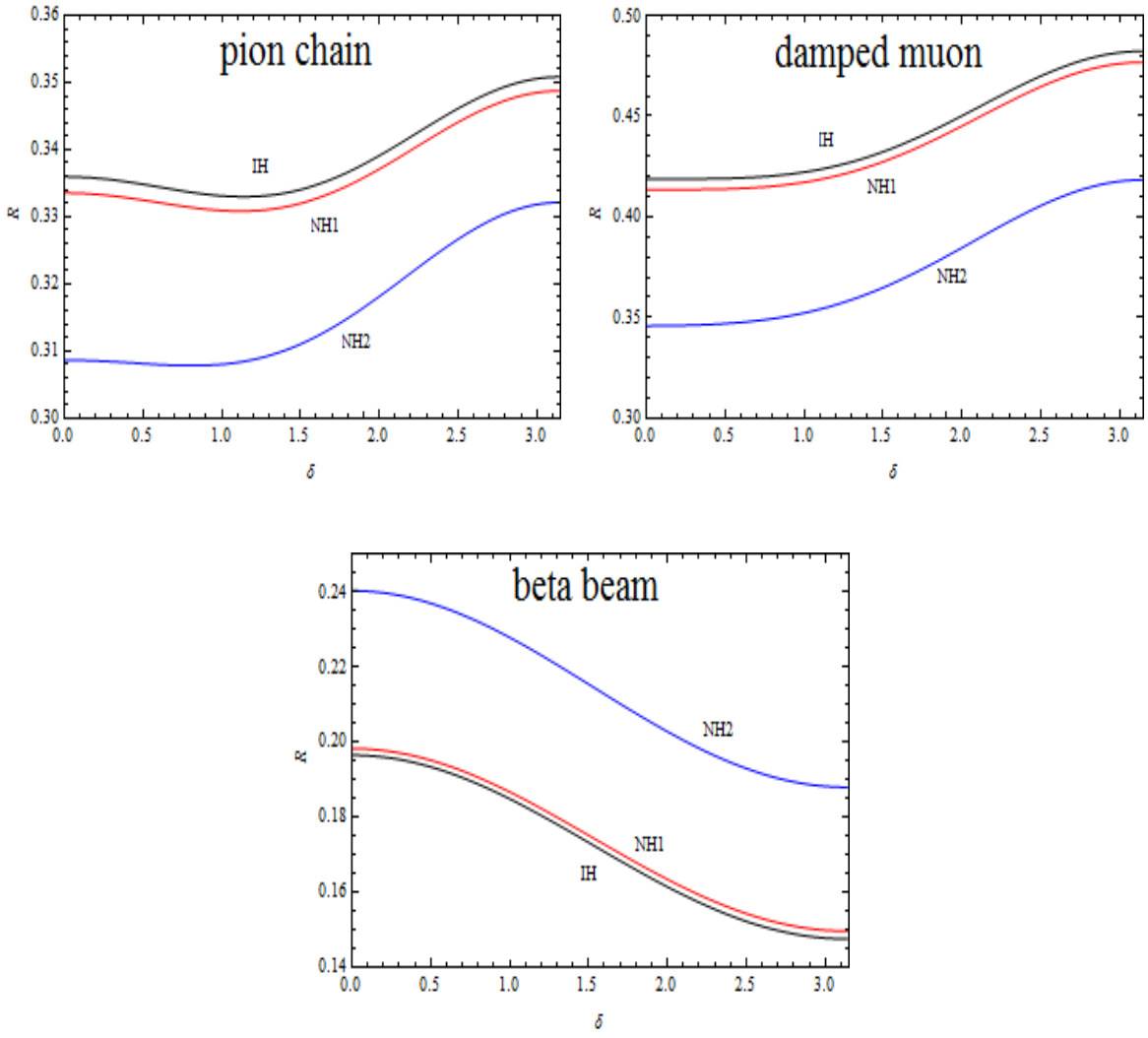

Figure III.1: R against δ for pion-chain, damped-muon and beta-beam injection models.

III.3.1 Three Popular Injection Models

In each of the three popular injection models, we calculate R for NH1, NH2 and IH. The three figures in Fig. III.1 display R against δ for pion-chain, damped-muon and beta-beam injection models respectively. From Fig. III.1, it is obvious that the fluctuation of R with varying δ is small in the pion-chain case while relatively large in the other two cases. For instance, we have $0.3 < R < 0.35$ for pion-chain, $0.35 < R < 0.5$ for damped-muon and $0.14 < R < 0.25$ for beta-beam. In particular, completely independent of δ, NH1, NH2 and IH, these three injection models lead to distinctive ranges of R. This interesting

feature allows us to distinguish between these three injection models in the near future when neutrino telescopes have observed statistically sufficient number of events such that a conclusive value of R could be established.

In all of the three injections models, it is difficult to distinguish NH1 from IH. However, the differences between NH2 and IH in these injection models could be more significant. For instance, in the pion-chain case, the difference in R between NH2 and IH is at least 0.02. The typical differences in R between NH2 and IH in damped-muon and beta-beam cases are 0.06 and 0.04 respectively. Most importantly, the magnitudes of the differences in R between NH2 and IH in all of these three injection models are almost independent of the undetermined values of δ.

Therefore, when the neutrino telescopes can achieve the sensitivities in R down to about 0.02 or lower, we may be able to probe the mass hierarchies NH2 and IH by measuring the cosmic neutrino flavor ratios at the detectors. It is noteworthy that this scheme does not depend on a precise measurement of the Dirac CP-violating phase. The prelude to probing mass hierarchy by cosmic neutrino flavor ratios is the determination of the relevant injection model by establishing a conclusive value for R at neutrino telescopes.

III.3.2 The General Injection Model

In reality, it is possible that there are some deviations from pion-chain, damped-muon and beta-beam injection models which have exact initial neutrino flavor compositions. Of course, if the deviations from these three popular injection models are perturbatively small, then the previous results and conclusions would be sufficiently reliable. We don't know yet whether the deviations are small, so it is useful to study the general injection model. With one more free parameter α now, we will display a 3D plot with x-axis, y-axis and z-axis being α, δ and R respectively.

Since we are interested in the prospects of using the cosmic neutrino flavor ratios to probe mass hierarchy, it would be illuminating to investigate the difference $|R_{\rm IH} - R_{\rm NH2}|$ as

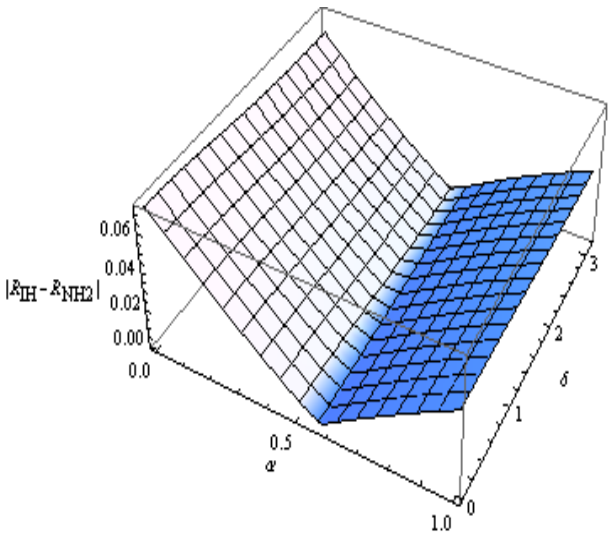

Figure III.2: The difference $|R_{\rm IH} - R_{\rm NH2}|$ as a function of both α and δ.

a function of both α and δ. We neglect the difference $|R_{\rm IH} - R_{\rm NH1}|$ because it is close to zero. In Fig. III.2, we see that $|R_{\rm IH} - R_{\rm NH2}|$ can be as large as 0.07. The magnitude depends mainly on α and is almost independent of δ. It is especially small when the injection model has roughly equal ν_e and ν_μ initial compositions ($\alpha \approx 1/2$). Hence, unless α is close to 1/2, neutrino telescopes will have the potential to distinguish NH2 from IH when they achieve the sensitivities in R down to about 0.02 or lower.

Currently, both T2K [51] and NOνA [52] are trying to measure δ precisely. It is possible that a reliable value for δ is ready by the time when neutrino telescopes have observed a statistically sufficient number of events to establish a conclusive value for R. If so, we could then reduce the 3D plots to 2D plots with R against α. (Actually, since $|R_{\rm IH} - R_{\rm NH2}|$ depends mainly on α and is almost independent of δ, we could have plotted R against α with δ fixed to be a random value. While this might be sufficiently illuminating, we kept those 3D plots for precise analyses.) Again, when neutrino telescopes have acquired sufficient sensitivities, they will be able to probe the mass hierarchy for the general injection model.

III.3.3 Caveats

In the analyses conducted above, we have adopted the recent global best-fit data of three neutrino mixing provided by [48]. The best-fit data indicate three possible cases, namely NH1, NH2 and IH. Based on this feature, we have shown that neutrino telescopes can distinguish between NH2 and IH once they have reached the sufficient sensitivities. If this feature persists in the forthcoming more precise global neutrino data-fittings, our scheme will remain a promising one.

III.4 Flavor Ratios and Mass Hierarchy: Beyond Standard Scenario

III.4.1 Active-Sterile Mixing

Short baseline neutrino experiments such as LSND [53] and MiniBooNE [54] seem to suggest the existence of eV-scale sterile neutrinos. Although the stringent bound from PLANCK satellite [55], taken at its face value, disfavors eV-scale sterile neutrinos, there are promising ways to reconcile their existence with cosmology [56; 57]. So it would be interesting to study the active-sterile mixing scenario.

To include the eV-scale sterile neutrinos, we adopt the parameterization and fits for the minimal 3+2 neutrino model found in [58]. It is quite straightforward to extend the 3×3 case to 5×5 one with the new fit values of $|U_{\alpha j}|$ plugged in:

$$|U_{e4}| = 0.149,\ |U_{e5}| = 0.127,\ |U_{\mu 4}| = 0.112,\ |U_{\mu 5}| = 0.127 \quad (\mathrm{NH}), \tag{III.10}$$

$$|U_{e4}| = 0.139,\ |U_{e5}| = 0.122,\ |U_{\mu 4}| = 0.138,\ |U_{\mu 5}| = 0.107 \quad (\mathrm{IH}). \tag{III.11}$$

However, the contributions from these new extra terms to the original values in $P_{\alpha\beta}$ are only of order $\sin^4\theta_{13}$ (0.024^2). These are negligible compared to the original P matrix elements at the order of $\sin\theta_{13}$ [7]. Therefore, our scheme is not affected by the active-sterile mixing.

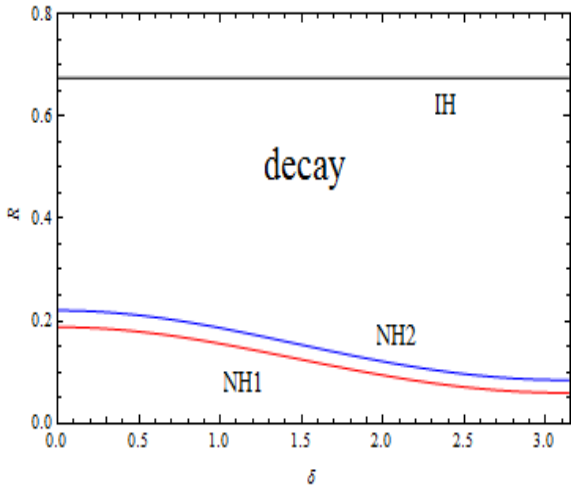

Figure III.3: R against δ for neutrino decay.

III.4.2 Neutrino Decay

It is possible that neutrinos decay in the following manner [17; 59]:

$$\nu_i \to \nu_j + X \quad \text{and} \quad \nu_i \to \bar{\nu}_j + X\,, \tag{III.12}$$

where X is a very light or massless particle such as a Majoron.

The value of R will be greatly altered if cosmic neutrinos from distant astrophysical sources decay. For simplicity, we assume that all the decays are complete and there is no other new physics besides decay. Regardless of any injection models, the final remnants are ν_1 in NH and ν_3 in IH. Thus, one can easily get [60]:

$$R = \frac{p_{\rm CC}\,|U_{\mu 1}|^2}{p_{\rm NC}\,|U_{\mu 1}|^2 + |U_{e1}|^2 + |U_{\tau 1}|^2} \qquad (\text{NH})\,, \tag{III.13}$$

$$R = \frac{p_{\rm CC}\,|U_{\mu 3}|^2}{p_{\rm NC}\,|U_{\mu 3}|^2 + |U_{e3}|^2 + |U_{\tau 3}|^2} \qquad (\text{IH})\,. \tag{III.14}$$

From Fig. III.3, it is clear that if we observe a track-event dominated ratio ($R \sim 0.65$), it would strongly indicate neutrino decay with IH, regardless of the undetermined values of δ. If we observe $0.25 < R < 0.65$, neutrino decay is disfavored. An observation of

a shower-event dominated ratio ($0.05 < R < 0.25$) may favor neutrino decay with NH. Recall that the beta-beam injection model (see Fig. III.1) predicts $0.14 < R < 0.25$ for both of NH and IH. Thus, neutrino decay with NH would be strongly favored if we observe $0.05 < R < 0.14$.

Among the 37 events detected by IceCube up until 2013, 9 events are tracks and 28 events are showers [61]. The expected background events are 8.4 ± 4.2 muon events and $6.6^{+5.9}_{-1.6}$ atmospheric neutrinos. Taking the best-fit values of 8.4 muon events and 6.6 atmospheric neutrinos, we obtain

$$R \sim \frac{9 - p_{\rm CC}\,(\frac{20}{21})\,(6.6) - 8.4}{28 - p_{\rm NC}\,(\frac{20}{21})\,(6.6) - (\frac{1}{21})\,(6.6)} \sim -0.151\,, \tag{III.15}$$

where the factors $20/21$ and $1/21$ are due to the fact that atmospheric neutrinos have the flavor ratio of $(\nu_e : \nu_\mu : \nu_\tau) \sim (1 : 20 : 0)$ at energy around 100 TeV. A negative R is disastrous. One might alleviate this issue by allowing the background events to take their minimum values, namely 4.2 muon events and 5.0 atmospheric neutrinos. In that case, we obtain $R \sim 0.052$. According to our discussions above, it appears that neutrino decay with NH is favored. Indeed, neutrino decay has been invoked to explain the apparent deficit of ν_μ events predicted by the pion-chain and damped-muon injection models at IceCube [62; 63; 64]. However, either $R \sim -0.151$ or $R \sim 0.052$ is not a statistically significant value at the moment. More events from IceCube are required to settle this value and more careful analysis [65] is also needed to draw a decisive conclusion.

III.4.3 Pseudo-Dirac Neutrinos

Neutrinos may be pseudo-Dirac states such that each generation is actually composed of two maximally-mixed Majorana neutrinos separated by a small mass difference [18; 66]. In this scenario, the only new parameters introduced are the three pseudo-Dirac neutrino mass differences, $\delta m_j^2 = (m_j^+)^2 - (m_j^-)^2$. While such neutrinos are indistinguishable from Dirac neutrinos in most cases due to the smallness of δm_j^2, they lead to an oscillatory and

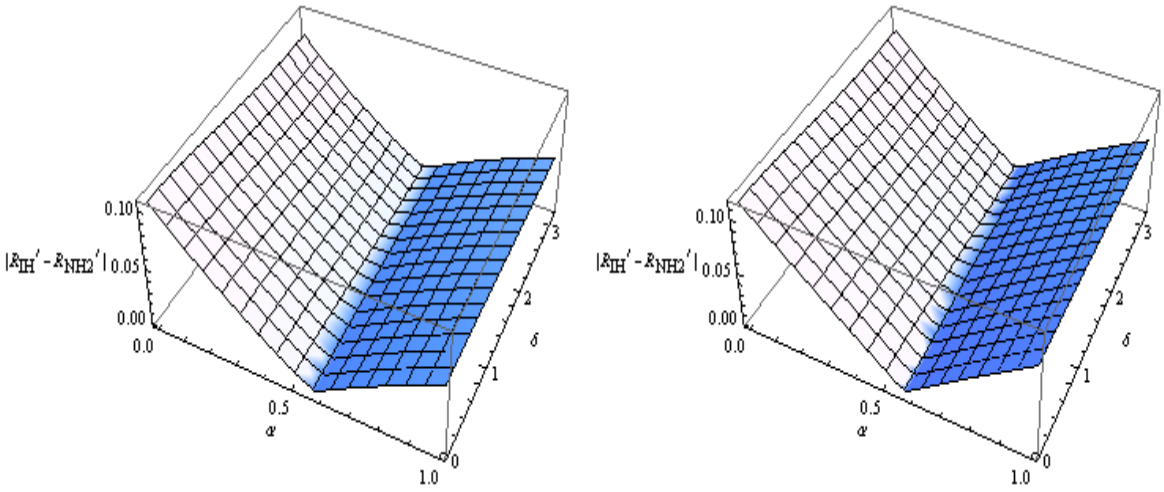

Figure III.4: The difference $|R'_{\rm IH} - R'_{\rm NH2}|$ as a function of both α and δ for pseudo-Dirac neutrinos. The left and right plots correspond to the parameter sets $\{\chi_1 = 0, \chi_2 = \frac{1}{2}, \chi_3 = \frac{1}{2}\}$ and $\{\chi_1 = \frac{1}{2}, \chi_2 = \frac{1}{2}, \chi_3 = 0\}$ respectively.

flavor-dependent reduction in flux. Flavor compositions are modified from the standard value of ϕ_β by the amount $\delta\phi_\beta = -\Delta_\beta\,\phi_\beta$ with

$$\Delta_\beta = |U_{\beta 1}|^2\,\chi_1 + |U_{\beta 2}|^2\,\chi_2 + |U_{\beta 3}|^2\,\chi_3\,, \tag{III.16}$$

where $\chi_j = \sin^2(\,\delta m_j^2 L/4E)$ can be either $\frac{1}{2}$ or 0 after statistical average, depending on whether δm_j^2 is accessible or not. The track-to-shower ratio becomes

$$R' = \frac{p_{\rm CC}\,(1-\Delta_\mu)\,\phi_\mu}{p_{\rm NC}\,(1-\Delta_\mu)\,\phi_\mu + (1-\Delta_e)\,\phi_e + (1-\Delta_\tau)\,\phi_\tau}\,. \tag{III.17}$$

We have explored different combinations of $\{\chi_1, \chi_2, \chi_3\}$ by studying 3D plots with axes being α, δ and R'. For $\{\chi_1 = \frac{1}{2},\ \chi_2 = 0$ or $\frac{1}{2}, \chi_3 = 0\}$ and $\{\chi_1 = 0,\ \chi_2 = 0$ or $\frac{1}{2}, \chi_3 = \frac{1}{2}\}$, we find $R' > R$ and $R' < R$ respectively. The range of enhancement and reduction with respect to R can be summarized as $0 \lesssim |R' - R| \lesssim 0.1$. For $\chi_1 = \chi_3$, we obtain $R' \approx R$. The above statements are valid for any injection model, mass hierarchy and δ.

In Fig. III.4, we display the 3D plots corresponding to $\{\chi_1 = 0, \chi_2 = \frac{1}{2}, \chi_3 = \frac{1}{2}\}$ and $\{\chi_1 = \frac{1}{2}, \chi_2 = \frac{1}{2}, \chi_3 = 0\}$. Comparing these two plots with Fig. III.2, one can see

that $|R'_{\rm IH} - R'_{\rm NH2}| > |R_{\rm IH} - R_{\rm NH2}|$ and the difference could be as large as 0.03. Thus, for these two cases, pseudo-Dirac neutrinos require lower sensitivities at neutrino telescopes to distinguish NH2 from IH. For all other combinations of $\{\chi_1, \chi_2, \chi_3\}$, we find that $|R'_{\rm IH} - R'_{\rm NH2}|$ has almost the same magnitude as $|R_{\rm IH} - R_{\rm NH2}|$ for any given injection model and δ. In other words, the corresponding 3D plots for $|R'_{\rm IH} - R'_{\rm NH2}|$ in these cases appear very similar to the one shown in Fig. III.2 and so we do not display them.

III.5 Conclusions

In this chapter, we have studied the cosmic neutrino flavor ratios against the undetermined Dirac CP-violating phase at neutrino telescopes. As a consequence, we have demonstrated how to probe mass hierarchy (NH or IH) at neutrino telescopes by the precise measurements of the cosmic neutrino flavor ratios. Our scheme is based on the global neutrino data fitting by [48] whose best-fit data suggest the possibilities of NH1 with $\theta_{23} > \pi/2$, NH2 with $\theta_{23} < \pi/2$ and IH with $\theta_{23} > \pi/2$.

We have investigated the pion-chain, damped-muon and beta-beam injection models in detail. Since it is possible that there are some deviations from these three idealized models, we have also studied the general injection model. We have shown that unless the injection model has roughly equal ν_e and ν_μ initial compositions ($\alpha \approx 1/2$), we should be able to distinguish NH2 from IH when the neutrino telescopes could measure the track-to-shower ratio R with the sensitivities down to about 0.02 or lower. The sensitivities required are independent of the undetermined values of the Dirac CP-violating phase.

Moreover, we have explored the possible effects of active-sterile mixing, neutrino decay and pseudo-Dirac nature of neutrinos. Since the active-sterile mixing is small, our scheme is completely not affected by it. A distinctive feature of neutrino decay is that if we observe $0.05 < R < 0.14$ ($R \sim 0.65$), it would strongly indicate neutrino decay with NH (IH), regardless of the undetermined values of δ. If neutrinos are pseudo-Dirac, there are many possibilities. However, for most of the possible combinations of $\{\chi_1, \chi_2, \chi_3\}$, the

sensitivities at neutrino telescopes required to distinguish NH2 from IH are almost the same as those in the standard scenario for any injection model and δ. The only exceptions are $\{\chi_1 = 0, \chi_2 = \frac{1}{2}, \chi_3 = \frac{1}{2}\}$ and $\{\chi_1 = \frac{1}{2}, \chi_2 = \frac{1}{2}, \chi_3 = 0\}$ where the required experimental sensitivities are lower than those in the standard scenario.

Undoubtedly, the observation of 37 neutrino events at IceCube represents the beginning of the era of neutrino astronomy. The recently deployed Antares [10] or the soon-to-be deployed KM3NeT [11] may also observe cosmic neutrinos and provide complimentary results for determining the cosmic neutrino flavor ratios on Earth. Furthermore, the proposed expansion of IceCube, if approved, will significantly increase its sensitivity to the composition of cosmic neutrinos. With the combined effort of these experiments, probing mass hierarchy at neutrino telescopes may become a realistic alternative to LBNE, PINGU and JUNO.

CHAPTER IV

Glashow Resonance as a Window into Cosmic Neutrino Sources

IV.1 Background

The rate of interaction of ν_e, ν_μ, ν_τ, $\bar{\nu}_\mu$, $\bar{\nu}_\tau$, with electrons is mostly negligible compared to interactions with nucleons. However, the case of $\bar{\nu}_e$ is unique because of resonant scattering, $\bar{\nu}_e e^- \to W^- \to$ anything, at $E_\nu \simeq 6.3$ PeV. The W^- resonance in this process is commonly referred to as the Glashow resonance [67]. The signal for $\bar{\nu}_e$ at the Glashow resonance, when normalized to the total $\nu + \bar{\nu}$ flux, can be used to differentiate among the main primary mechanisms for neutrino-producing interactions in optically thin sources of cosmic rays [68].

In 2012, IceCube released the first two-year equivalent dataset, observing high-energy non-atmospheric neutrino events for the first time [3; 40]. The maximum neutrino energy inferred was 1–2 PeV. In 2014, IceCube reported its three-year dataset [61]. The maximum neutrino energy inferred to date remains at ~ 2 PeV. The energy resolution on the observed events is $\sim 25\%$. In particular, Glashow resonance events should produce showers that are not (yet) observed. The integrated cross section of the resonance is comparable for some flavor models to that of the non-resonant spectrum integrated above a PeV, which implies that the falling power law ($E_\nu^{-\alpha}$) of the incident neutrino spectrum is effectively canceled and that resonant events could have been seen [69].

In this work, we evaluate the ratio of the expected number of Glashow events at 6.3 PeV to the number of non-resonant events expected above various minimum energies ($\sim$ PeV) for six popular cosmic neutrino source models.

IV.2 Six Astrophysical Neutrino Source Models

We consider six possible source models:

(i) $pp \to \pi^\pm$ pairs $\to \nu_e + \bar{\nu}_e + 2\nu_\mu + 2\bar{\nu}_\mu$, referred to as the *"$\pi^\pm$ mode"*;

(ii) $pp \to \pi^{\pm}$ pairs $\to \nu_\mu,\ \bar{\nu}_\mu$ only, referred to as the *"damped $\mu^{\pm}$ mode"*;

(iii) $p\gamma \to \pi^{+}$ only, $\to \nu_e + \nu_\mu + \bar{\nu}_\mu$, referred to as the *"$\pi^{+}$ mode"*;

(iv) $p\gamma \to \pi^{+} \to \nu_\mu$ only, referred to as the *"damped μ^{+} mode"*;

(v) charm production and immediate decay to $\nu_e,\ \bar{\nu}_e,\ \nu_\mu,\ \bar{\nu}_\mu$, referred to as the *"prompt mode"*; and

(vi) β-decay of cosmic neutrons to $\bar{\nu}_e$, referred to as the *"neutron decay (or β decay) mode"*.

The initial flavor content of the produced neutrinos in these six models are summarized in the second column of Table IV.1.

Table IV.1: Neutrino flavor ratios at source, component of $\bar{\nu}_e$ in total neutrino flux at Earth after mixing and decohering, and consequent relative strength of Glashow resonance, for six astrophysical models. (Neutrinos and antineutrinos are shown separately, when they differ.)

	Source flavor ratio		Earthly flavor ratio		$\bar{\nu}_e$ fraction in flux ($\mathscr{R}$)
$pp \to \pi^{\pm}$ pairs	(1:2:0)		(1:1:1)		$18/108 = 0.17$
w/ damped $\mu^{\pm}$	(0:1:0)		(4:7:7)		$12/108 = 0.11$
$p\gamma \to \pi^{+}$ only	(1:1:0)	(0:1:0)	(14:11:11)	(4:7:7)	$8/108 = 0.074$
w/ damped μ^{+}	(0:1:0)	(0:0:0)	(4:7:7)	(0:0:0)	0
charm decay	(1:1:0)		(14:11:11)		$21/108 = 0.19$
neutron decay	(0:0:0)	(1:0:0)	(0:0:0)	(5:2:2)	$60/108 = 0.56$

When the $\pi^{\pm}$ mode occurs in an astrophysical source, isospin invariance yields a roughly

equal ratio of π^+, π^-, and π^0 production, followed by decay of the charged $\pi^\pm$s through the $\mu^\pm$ chain to produce equal numbers of ν_μ and $\bar{\nu}_\mu$, a number of ν_e plus $\bar{\nu}_e$ equal to a half of ν_μ plus $\bar{\nu}_\mu$, and roughly equal numbers of ν_e and $\bar{\nu}_e$. The rest-frame lifetimes of the charged pions and muons are 2.6×10^{-8} s and 2.2×10^{-6} s, respectively. Since the rest frame lifetime of the muon exceeds that of the charged pion by a factor of 85, it is possible for $\pi^\pm$ decay to take place but the subsequent $\mu^\pm$ decay to be inhibited [15]. This would happen if the muon in the decay chain loses energy in the source environment before it decays (e.g., by synchrotron radiation in a $\vec{B}$-field, or by scattering). In a falling spectrum, the decay of a lower-energy muon would make a negligible contribution. This damped $\mu^\pm$ mode results in only ν_μ and $\bar{\nu}_\mu$ being produced at the source; flavor mixing between the source and Earth then produces a small amount of $\bar{\nu}_e$.

In contrast to charged-pion production by pp scattering, charged pions may be produced by $p\gamma$ scattering. Here, the Δ^+ resonance contributes to produce $\pi^+ + n$ and $\pi^0 + p$, in the ratio of 1 : 2. Since π^- production is suppressed and the π^+ mode produces no $\bar{\nu}_e$s at the source, only a small amount of $\bar{\nu}_e$ arises from mixing [68]. If, in addition, the μ^+s in $p\gamma$ mode are damped, then no antineutrinos are produced at all at the source, and so even with mixing there will be no $\bar{\nu}_e$s at Earth.

Charmed particles decay promptly (e.g. the $D^\pm$ has a lifetime of 1.0×10^{12} s) and semileptonically to $e^\pm$ or $\mu^\pm$ (e.g., the $D^\pm$ has a 34% branching ratio to these modes). Lepton universality ensures that equal numbers (modulo small mass differences) of ν_e, $\bar{\nu}_e$, ν_μ, and $\bar{\nu}_\mu$ are produced, while production of ν_τ and $\bar{\nu}_\tau$ is kinematically suppressed. Thus, $\bar{\nu}_e$s produced in charm decay will arrive at Earth.

Finally, there may be sources that inject a nearly pure neutron flux [14]. Such would be the case if Fe is emitted and subsequently dissociated to protons and neutrons, with the charged protons then degraded in energy, or swept aside, by a magnetic field at the source. Such would also be the case if the cosmic accelerator entrains and accelerates charged protons, with cosmic-ray escape occurring via $p_{\rm entrained} \rightarrow n + \pi^+$. This escaping (and

pointing) beta beam decays to pure $\bar{\nu}_e$, leading to a large amount of $\bar{\nu}_e$ arriving at Earth, even after mixing.

Each of these six models are possible, as are combinations of the six. For our purposes, we consider each model in isolation, and show how the rate for Glashow resonant events can serve as a barometer ("resonometer") distinguishing among these six source models. A caveat is in order here. It has been shown, especially in Ref. [16], that multi-pion contributions can produce antineutrinos which via mixing ensure some $\bar{\nu}_e$s at Earth. These multi-pion contributions are not included in our discussion here. For certain source parameters, the "contamination" from multi-pion processes can be large. In addition, we assume that possible damping of muons at the sources is complete; it may be incomplete, in which case results will be intermediate between the cases considered here. We also do not consider neutrino absorption by the Earth, which can be conservable for upcoming $\bar{\nu}_e$. We mention in passing that the effect of kaon decays on source neutrino flavor ratios is small in the energy range of interest [16]. All in all, our results must be treated as suggestive. If Glashow resonance events are observed, a more careful treatment than presented here will be warranted. Until Glashow resonance events are observed, our results can be considered motivational.

At this early stage of astrophysical data collection, it is a good approximation [7] to assume that tribimaximal mixing [13] holds. Then, the evolution $\nu_\alpha \to \nu_\beta$, with α and β any elements of the three-flavor set $\{e,\ \mu,\ \tau\}$, is described in terms of the PMNS matrix U, by the symmetric propagation matrix P whose positive definite elements are

$$P_{\alpha\beta} = \sum_j |U_{\alpha j}|^2 \, |U_{\beta j}|^2 = \frac{1}{18} \begin{pmatrix} 10 & 4 & 4 \\ 4 & 7 & 7 \\ 4 & 7 & 7 \end{pmatrix} . \tag{IV.1}$$

The element with the largest uncertainty is $P_{e\mu}$, which has an uncertainty of 20% at 2σ. From the last column of Table IV.1, we see that all but one of the fifteen combinations of

the six flux models predict a difference much larger than 20% for the $\bar{\nu}_e$ fraction.

IV.3 Resonant and Non-resonant events

The resonant cross section for $\bar{\nu}_e + e^- \to W^- \to$ hadrons is

$$\sigma_{\rm Res}(s) = 24\pi\Gamma_W^2\ {\rm B}(W^- \to \bar{\nu}_e e^-)\,{\rm B}(W^- \to {\rm had})\frac{(s/M_W^2)}{(s-M_W^2)^2+(M_W\Gamma_W)^2}\,, \qquad \text{(IV.2)}$$

where M_W is the W mass (80.4 GeV), Γ_W is the W's FWHM (2.1 GeV), and ${\rm B}(W^- \to \bar{\nu}_e e^-)$ and ${\rm B}(W^- \to {\rm had})$ are W^- branching ratios to the $\bar{\nu}_e e^-$ state (11%) and the hadronic state (67%), respectively. At the peak,

$$\sigma_{\rm Res}^{\rm peak}(s) = \frac{24\pi\,{\rm B}(W^- \to \bar{\nu}_e e^-)\,{\rm B}(W^- \to {\rm had})}{M_W^2} = 3.4\times10^{-31}{\rm cm}^2\,. \qquad \text{(IV.3)}$$

Consequently, the resonant cross section may be written as

$$\sigma_{\rm Res} = \left[\frac{\Gamma_W^2\, s}{(s-M_W^2)^2+(M_W\Gamma_W)^2}\right]\sigma_{\rm Res}^{\rm peak}(s)\,. \qquad \text{(IV.4)}$$

The W's width is small compared to the W's mass ($\frac{\Gamma_W}{M_W} = 2.6\%$), and the experimental resolution will always exceed by far the W width. Thus, we are justified in using the "narrow width approximation" (NWA) throughout. A contour integration in s over the s-dependent bracketed expression in Eq. (IV.4), and the residue theorem, yields the value $\pi M_W\Gamma_W$. Thus, the resulting NWA is simply

$$\sigma(s)_{\rm Res} = (\pi M_W\Gamma_W)\,\sigma_{\rm Res}^{\rm peak}(s)\,\delta(s-M_W^2)\,, \qquad \text{(IV.5)}$$

and the number of resonant events per unit time and unit steradian is

$$\left(\frac{N}{T\Omega}\right)_{\rm Res} = N_e\,(\pi M_W\Gamma_W)\,\sigma_{\rm Res}^{\rm peak}\int dE_{\bar\nu_e}\left(\frac{dF_{\bar\nu_e}}{dE_{\bar\nu_e}}\right)\delta(s-M_W^2)$$

$$= \frac{N_p}{2m_e}\,(\pi M_W\Gamma_W)\,\sigma_{\rm Res}^{\rm peak}\left.\frac{dF_{\bar\nu_e}}{dE_{\bar\nu_e}}\right|_{E_{\bar\nu_e}=6.3{\rm PeV}}, \qquad \text{(IV.6)}$$

where $N_e = N_p$ is the number of electrons or protons in the detector volume.

In contrast, the continuum (non-resonant) neutrino event rate between $E_\nu^{\rm min} \sim$ PeV to $E_\nu^{\rm max}$ is given by

$$\begin{aligned}\left(\frac{N}{T\Omega}\right)_{\rm non-Res} &= N_{n+p}\int_{E_\nu^{\rm min}}^{E_\nu^{\rm max}} dE_\nu\left(\frac{dF_\nu}{dE_\nu}\right)\sigma_{\nu N}^{\rm CC}(E_\nu)\\ &\approx \frac{N_{n+p}}{(\alpha-1.40)}\left[\left(\sigma_{\nu N}^{\rm CC}\,E_\nu\left(\frac{dF_\nu}{dE_\nu}\right)\right)\Big|_{E_\nu^{\rm min}} - \left(\sigma_{\nu N}^{\rm CC}\,E_\nu\left(\frac{dF_\nu}{dE_\nu}\right)\right)\Big|_{E_\nu^{\rm max}}\right]\\ &= \frac{N_{n+p}}{(\alpha-1.40)}\left[\left(\frac{6.3\,{\rm PeV}}{E_\nu^{\rm min}}\right)^{(\alpha-1.40)} - \left(\frac{6.3\,{\rm PeV}}{E_\nu^{\rm max}}\right)^{(\alpha-1.40)}\right]\\ &\quad\times\left(\sigma_{\nu N}^{\rm CC}(E_\nu)\frac{E_\nu\,dF_\nu}{dE_\nu}\right)\Big|_{E_\nu=6.3\,{\rm PeV}}, \qquad \text{(IV.7)}\end{aligned}$$

where N_{n+p} is the number of nucleons in the detector volume, and $\frac{dF_\nu}{dE_\nu}$ is the total (summed over flavors) ν plus $\bar\nu$ flux. Here we have assumed an $E^{0.40}$ energy dependence for $\sigma_{\nu N}$ as predicted for the 1–10 PeV region in Ref. [70], and we have included only the charged-current cross section; in a falling spectrum, the neutral-current contribution is lower in average by $\frac{\sigma_{\nu N}^{NC}(E_{\rm obs})}{\sigma_{\nu N}^{CC}(E_{\rm obs})}\langle y\rangle^{\alpha-0.4}$, where $\langle y\rangle = \frac{E_{\rm obs}}{E}$ is the average fraction of energy transferred from the incident neutrino to the detector. The simple Fermi shock-acceleration mechanism yields $\alpha = 2.0$, whereas an earlier statistical study of the first-release dataset concluded that α was constrained by the absence of Glashow events in the IceCube data to $\alpha \geq 2.3$ [71; 2]. Taking $\langle y\rangle \sim 0.25$ and the NC to CC ratio to be 0.4, one finds less than a 5% contribution from the neutral-current even with the conservative spectral index of $\alpha = 2$.

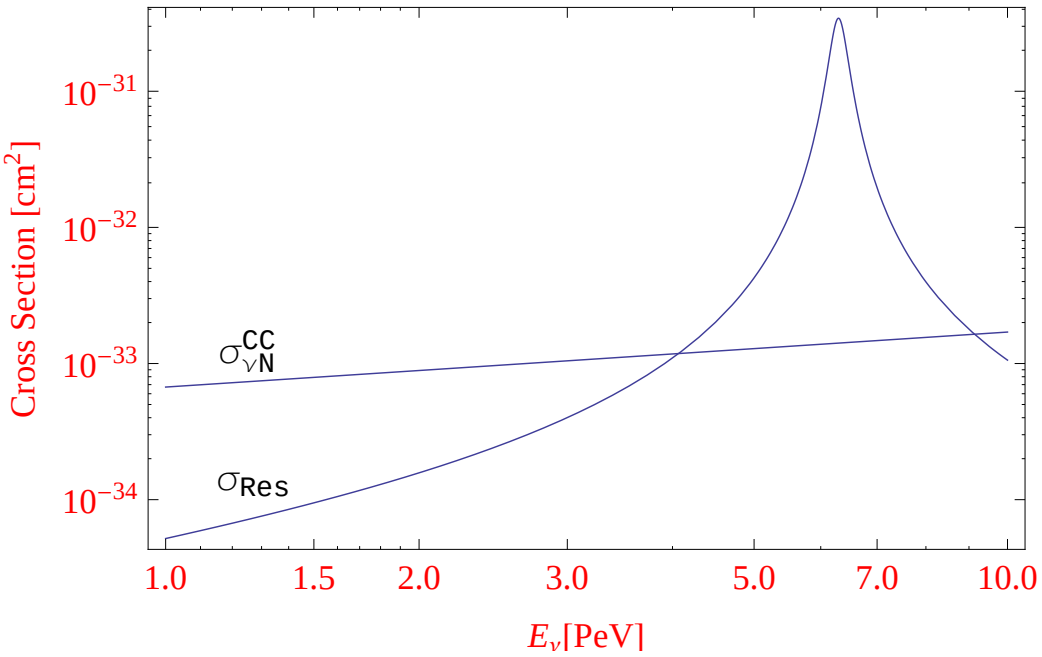

Figure IV.1: Cross sections for the resonant process, $\bar{\nu}_e + e^- \to W^- \to$ hadrons, and the non-resonant process, $\nu_e + N \to e^- +$ hadrons, in the 1–10 PeV region.

The resonant cross section and the non-resonant charged-current $\sigma_{\nu_{eN}}$ cross section are shown in Fig. IV.1.

From Eq. (IV.7), it is seen that the integrated continuum event rate scales with the minimum energy as

$$\left(\frac{N}{T\Omega}\right)_{\text{non}-\text{Res}} \propto \left[(E_\nu^{\text{min}})^{-(\alpha-1.40)} - (E_\nu^{\text{max}})^{-(\alpha-1.40)} \right] . \tag{IV.8}$$

Failure of future events to follow this energy-dependent rate equation would indicate a broken power-laaw spectrum, or in the extreme case, a cutoff spectrum. On the other hand, when E_ν^{max} can be taken to infinity, as can be done when the neutrino energy spectrum is a power-law falling as fast or faster than E^{-2}, then we count all events that are initiated in the IceCube detector with energy exceeding E_ν^{min}.

We normalize the expected number of events in any energy interval to the expected number $\langle N_{\text{1-2 PeV}}^{\text{expected}} \rangle$ for the highest-energy IceCube bin with nonzero number, the 1-2 PeV

bin. Then, in the limit $E_\nu^{\rm max} \to \infty$, we have that the expected number of continuum events above $E_\nu^{\rm min}$ is

$$N^{\rm expect}(\geq E_\nu) = \left(\frac{E_\nu^{-(\alpha-1.40)}}{1-2^{-(\alpha-1.40)}} \right) \langle N^{\rm expected}_{\text{1-2 PeV}} \rangle \,, \tag{IV.9}$$

which for $\alpha = 2.0$ and 2.3 is equal to $2.94\,E^{-0.6}\,\langle N^{\rm expected}_{\text{1-2 PeV}} \rangle$ and $2.15\,E^{-0.9}\,\langle N^{\rm expected}_{\text{1-2 PeV}} \rangle$, respectively. In turn, the number expected above 1 PeV is $2.94\,\langle N^{\rm expected}_{\text{1-2 PeV}} \rangle$ and $2.15\,\langle N^{\rm expected}_{\text{1-2 PeV}} \rangle$, respectively; the number of events expected above 2 PeV is $1.94\,\langle N^{\rm expected}_{\text{1-2 PeV}} \rangle$ and $1.15\,\langle N^{\rm expected}_{\text{1-2 PeV}} \rangle$, respectively.

The 1-2 PeV IceCube bin contains the three observed events. The expected event number for this bin is not known. The "Feldman-Cousins" [72] tables provide an estimate for the range of expected numbers of events, given an observed number of events, with or without background. (The zero-background case is the relevant one for us.) Given three events in the 1-2 PeV bin, the Feldman-Cousins expected number of events for this bin is 0.82 to 8.25 at 95% C.L. However, there is additional information in the IceCube data: no events are observed above ~ 2 PeV. Thus, tension between the populated bin and the remaining unpopulated bins is minimized by investigating the lower numbers of expected events. Consider the integer expected values $\langle n \rangle = 1$, 2, and 3 as representative; the mean value 3 is appropriate if the observed value were spot on the mean, while the mean values 1 and 2 are appropriate if the observed value is an upward fluctuation. The Poisson probability to observe n events against an expected number $\langle n \rangle$ is $P(n|\langle n \rangle) = e^{-\langle n \rangle}\,\frac{\langle n \rangle^n}{n!}$. Thus, we have probabilities $P(3|3) = 22\%$ for the "spot-on" rate, and $P(3|2) = 18\%$ and $P(3|1) = 6.1\%$ for possible upward fluctuations. Since we discount the disfavored cases where $\langle n \rangle > n$, we do not have the general Poisson result that $\int_0^\infty d\langle n \rangle\, P(n|\langle n \rangle) = 1$. Thus, it is the relative rates 1, 0.82, and 0.28 for the expected values 3, 2, 1, respectively, that lead us to the obvious conclusion: with just three events, the unknown expected number spans a large range of possibilities and so is ill-determined.

For $\langle N^{\rm expected}_{\text{1-2 PeV}} \rangle = 3$, 2, 1, we expect $N(\geq 2\,\text{PeV}) = 5.8\,(3.5)$, $3.9\,(2.3)$, $1.9\,(1.15)$ events,

for $\alpha = 2.0$ (2.3), respectively. No events above ~ 2 PeV are observed. The Poisson probability for a downward fluctuation to no events in a bin where $\langle n \rangle$ are expected is $P(0|\langle n \rangle) = e^{-\langle n \rangle}$. Thus, the tension between observed events in the 1-2 PeV bin and the absence of events above 2 PeV is quantified in the probabilities to observe none of the expected continuum events above 2 PeV: 0.30% (3.0%), 2.0% (10%), and 15% (33%), respectively. Moreover, if one normalizes to the three observed events not in the 1-2 PeV interval, but rather in the 1-3 PeV interval, then the expected number of continuum events above 3 PeV is reduced to 3.2 (1.8), with Poisson probabilities to observe no events of 4.1% (17%). As discussed above, these odds are higher if the three observed events are themselves an upward fluctuation.

At face value, these results favor the more steeply falling spectrum, and may even suggest a broken power law or cutoff [73] in the neutrino spectrum. However, these results are not compelling at present.

Here we will assume that the absence of events is the result of a downward fluctuation, and continue the calculation with the unbroken power spectrum to assess possibilities for the Glashow resonance event rate. Since the event rate expected for the continuum and Glashow resonance depends on the expected rate determined with $\sim$PeV events, one cannot yet predict the number of expected events at higher energy. Nevertheless, in the ratio of expected Glashow events to expected continuum events, which we next present, the normalizing factor cancels out. This is not true for downcoming $\bar{\nu}_e$ events, where the absorption can be neglected.

From Eqs. (IV.6) and (IV.7), we find the ratio of resonant Glashow events to non-

resonant continuum events to be

$$\frac{N_{\rm Res}}{N_{\rm non-Res}(E_\nu > E_\nu^{\rm min})}$$
$$= \frac{10\,\pi}{18}\left(\frac{\Gamma_W}{M_W}\right)\left(\frac{\sigma_{\rm Res}^{\rm peak}}{\sigma_{\nu N}^{\rm CC}(E_\nu = 6.3\,{\rm PeV})}\right)\frac{(\alpha-1.40)\left(\frac{E_\nu^{\rm min}}{6.3\,{\rm PeV}}\right)^{\alpha-1.40}}{\left[1-\left(\frac{E_\nu^{\rm min}}{E_\nu^{\rm max}}\right)^{(\alpha-1.40)}\right]}\,\mathscr{R}\,, \qquad \text{(IV.10)}$$
$$= 11\times\frac{(\alpha-1.40)\left(\frac{E_\nu^{\rm min}}{6.3\,{\rm PeV}}\right)^{\alpha-1.40}}{\left[1-\left(\frac{E_\nu^{\rm min}}{E_\nu^{\rm max}}\right)^{(\alpha-1.40)}\right]}\times\mathscr{R}\,, \quad \text{with } \mathscr{R}\equiv\left[\left(\frac{dF_{\bar\nu_e}}{dE_{\bar\nu_e}}\right)/\left(\frac{dF_\nu}{dE_\nu}\right)\right]_{E=6.3\,{\rm PeV}}.$$

Here we have taken $\frac{N_p}{N_p+N_n} = \frac{10}{18}$ in the detector material (water), and set $\sigma_{\nu N}^{\rm CC} = \sigma_{\bar\nu_e N}^{\rm CC} = 1.42\times10^{-33}$ cm^2 at $E_\nu = 6.3$ PeV [70]. $\mathscr{R}$ is the ratio of the $\bar\nu_e$ flux that produces the resonance events to the total ν flux that produces the continuum events; $\mathscr{R}$ is a model-dependent number, exhibited for each of our six models in the final column of Table IV.1. We stress that the ratio in Eq. (IV.10) is valid for down-coming events, but not for up-coming events. The reason is that the large resonant cross section at 6.3 PeV implies that 6.3 PeV neutrinos are strongly absorbed if transiting the Earth, thereby eliminating the possibility for up-coming Glashow events [70].

We list in Table IV.2 the ratio of Glashow events to continuum events above $E_\nu^{\rm min} =$ 1, 2, 3, 4, 5 PeV, with $\alpha = 2.0$ (2.3) and $E_\nu^{\rm max} = \infty$, for the six models of cosmic neutrino production under consideration.[1] Note that we keep the value of $E_\nu^{\rm min}$ well below the energy region of the resonance: at the energy value of the peak minus one FWHM, the incident neutrino energy is $6.3\,{\rm PeV}\,(1-\Gamma_W/M_W)^2 \approx 6.3\,{\rm PeV}\,(1-0.052) = 6.0\,{\rm PeV}$.

We note that the numbers of expected resonant events presented in Table IV.2 is greatly reduced from the ratio of resonant to non-resonant cross sections by the additional factors. The cross section ratio at 6.3 PeV is 240: see Fig. IV.1. The $\frac{\Gamma_W}{M_W}$ ratio is 1/38. The α-

[1] The purpose of allowing for a finite $E_\nu^{\rm max}$ in Eq. (IV.10) is to compare our ratios to the ratios that result from the effective areas provided in Ref. [40]. There an $E_\nu^{\rm max} = 10$ PeV. On including this $E_\nu^{\rm max}$ in our calculation, we find very good agreement with the IceCube numbers. Note that in the IceCube nomenclature for incident $\nu+\bar\nu$ fluxes, the ratio of down-coming Glashow events to continuum events is given by $\left(\frac{\nu_e-\nu_\mu}{3\nu_\mu}\right)_{south}$.

dependent factor $\left[(\alpha - 1.40)\left(\frac{1\,\mathrm{PeV}}{6.3\,\mathrm{PeV}}\right)^{\alpha-1.40}\right]$ yields about 0.2 for both α's of interest, 2.0 and 2.3. The end result is about $2\mathscr{R}$ for the ratio of resonant events to non-resonant events above 1 PeV.

Of course, the expected number of Glashow events does depend on $\langle N^{\mathrm{expected}}_{1\text{-}2\,\mathrm{PeV}}\rangle$. The number of Glashow events is found by multiplying the first numerical column of Table IV.2 by $N(\geq 1\,\mathrm{PeV}) = 2.94\,\langle N^{\mathrm{expected}}_{1\text{-}2\,\mathrm{PeV}}\rangle$ $(2.15\,\langle N^{\mathrm{expected}}_{1\text{-}2\,\mathrm{PeV}}\rangle)$. These expected resonant event numbers are 1.1 (0.69), 0.71 (0.43), 0.47 (0.28), 0 (0), 1.2 (0.77), and 3.5 (2.1), each times $\langle N^{\mathrm{expected}}_{1\text{-}2\,\mathrm{PeV}}\rangle$, for the six models, and for $\alpha = 2.0\,(2.3)$. With increased statistics the Glashow event numbers may separate into values which discriminate among the astrophysical source models.

Since no 6.3 PeV events are observed, the Poisson probabilities for each model, based solely on the absence of resonance events, for $\langle N^{\mathrm{expected}}_{1\text{-}2\,\mathrm{PeV}}\rangle = 3$, are, 3.8% (13%), 12% (28%), 24% (43%), large (large), 2.7% (9.9%), and 0.0025% (0.18%), respectively; and for $\langle N^{\mathrm{expected}}_{1\text{-}2\,\mathrm{PeV}}\rangle = 1$, are 34% (50%), 49% (65%), 62% (76%), large (large), 30% (46%), 3.0% (12%), respectively. All models remain viable except perhaps the final one, where neutron decay to pure $\bar{\nu}_e$ predicts some resonance events at Earth. However, since the probabilities vary exponentially with $\langle N^{\mathrm{expected}}_{1\text{-}2\,\mathrm{PeV}}\rangle$, more data is needed before reasonably-definite conclusions can be drawn. These "Glashow-event" probabilities should be multipled by the continuum probabilities to determine overall Poisson probabilities for a $\langle N^{\mathrm{expected}}_{1\text{-}2\,\mathrm{PeV}}\rangle$ value, and for the unbroken power law hypotheses with $\alpha = 2.0$ and 2.3.

For the sake of completeness, we briefly consider the possibility of exotic neutrino properties that modify the flavor mix of neutrinos, specifically neutrino decay and pseudo-Dirac neutrino oscillations. Neutrino decay [17] allows the flavor mix to deviate significantly from the democratic mix. Observation of a significant $\bar{\nu}_e$ flux from SN1987A precludes any observable effects of ν_1 decay on L/E scales of astrophysical interest. In the case of a normal hierarchy (with mass ordering $m_{\nu_1} < m_{\nu_2} < m_{\nu_3}$), the ν_2 and ν_3 mass eigenstates may decay completely to ν_1, whose flavor content ratios are $|U_{e1}|^2 : |U_{\mu 1}|^2 : |U_{\tau 1}|^2 = 4 : 1 : 1$

Table IV.2: Ratio of resonant event rate around the 6.3 PeV peak to non-resonant event rate above $E_\nu^{\rm min} = 1,\ 2,\ 3,\ 4,\ 5$ PeV. The single power-law spectral index α is taken to be 2.0 and 2.3 for the non-parenthetic and parenthetic values, respectively. The single power-law extrapolation just above 1 PeV predicts a mean number of observed resonance events around 6.3 PeV, as calculated in the text.

$E_\nu^{\rm min}$ (PeV)	1	2	3	4	5
$pp \to \pi^\pm$ pairs	0.37 (0.32)	0.56 (0.59)	0.71 (0.85)	0.84 (1.1)	0.96 (1.3)
w/ damped $\mu^\pm$	0.24 (0.20)	0.37 (0.38)	0.47 (0.56)	0.54 (0.71)	0.62 (0.88)
$p\gamma \to \pi^+$ only	0.16 (0.13)	0.24 (0.26)	0.31 (0.37)	0.37 (0.48)	0.42 (0.59)
w/ damped μ^+	0 (0)	0 (0)	0 (0)	0 (0)	0 (0)
charm decay	0.41 (0.36)	0.62 (0.67)	0.80 (0.95)	0.94 (1.2)	1.1 (1.6)
neutron decay	1.2 (1.0)	1.9 (2.0)	2.3 (2.8)	2.8 (3.6)	3.2 (4.4)

for both ν and $\bar{\nu}$. The $\bar{\nu}_e$ content of the neutrino flux at Earth is then $1/3$ which may be an *enhancement*. On the other hand, if the mass hierarchy is inverted (with $m_{\nu_3} < m_{\nu_1} < m_{\nu_2}$), then both ν_1 and ν_3 are stable and a variety of final flavor ratios are possible, depending on the intial ratios of ν_1, ν_2, and ν_3, and the decay mode of ν_2.

Another possibility for deviations from standard flavor mixes [18] arises in scenarios of pseudo-Dirac neutrinos [74], in which each of the three neutrino mass eigenstates is a doublet with tiny mass differences less than 10^{-6} eV (to evade detection so far).[2] The smallness of the mass difference tells us that the mixing angle between the active state with $SU(2)$ couplings, and the sterile state without, is necessarily maximal. For cosmically-

[2] In fact, observing an energy-dependence of flavor mixes of high energy cosmic neutrinos is the only known way to detect mass-squared differences in the range $10^{-18} - 10^{-12}$ eV^2.

large L/E, the flux of each active flavor is therefore reduced by a half. Of course, if all three flavors are reduced by a half, there is no change in the flavor ratios; however, at intermediate energies each flavor can be reduced or not, leading to a possible suppression of the absolute flavor ratio for $\bar{\nu}_e$ by $R^{\rm pD}_{\bar{\nu}_e}/R_{\bar{\nu}_e}$ of roughly 1/2, or an enhancement of the $\bar{\nu}_e$ flux ratio of roughly 2. (Note that the maximal suppression/enhancement will be a bit less than 1/2 or 2 if there is a ν_e flux present.)

IV.4 Conclusions

Normalized to the three down-coming IceCube events in the 1-2 PeV range, we find that the number of predicted resonant Glashow events ranges from zero (for the damped μ^+ mode, which generates no antineutrinos) to almost three (for the neutron decay mode which generates only antineutrinos) times $\langle N^{\rm expected}_{\rm 1\text{-}2\,PeV}\rangle$. The other four popular neutrino-generating modes give intermediate values. Thus we have demonstrated that the fraction of resonance events is a potential discriminator among the popular neutrino-generating astrophysical models.

Our calculations are done in a somewhat idealized approximation. For example, in pion production from $p\gamma$ collisions, we consider only the contribution of the Δ^+ intermediate states. Also, we do not consider the possibility that more than one neutrino source model may be contributing. When more data become available, refinements on our "Resonometer" will become necessary.

Until that day, we conclude that the absence of Glashow resonance events in IceCube favors the lower values of the fractional $\bar{\nu}_e$ flux. Should this non-observation of resonance events continue, the "damped μ^+ mode" $p\gamma \to \pi^+ n \to n + \mu^+ + \nu_\mu$ would become uniquely favored.[3] Caveats to this conclusion include the possibility of pseudo-Dirac neutrino oscillations, and the possibility of neutrino decay.

[3] In Ref. [75] it was noted that a damped μ^+ mode will suppress antineutrinos and therefore the Glashow event rate, but will also generate in IceCube "double-bang" events in the $3-10$ PeV range via ν_μ oscillations to ν_τ's.

CHAPTER V

Aspects of the Flavor Triangle for Cosmic Neutrino Propagation

V.1 Overview of Cosmic Neutrino Flavors and Flavor Triangles

The IceCube neutrino telescope has begun observation of neutrinos from distant sources [61; 40]. It is expected that detections from the recently deployed Antares [10], and the soon-to-be deployed KM3NeT, will soon follow. After an ensemble of neutrino events have been collected, track versus shower topologies will allow one to extract a neutrino flavor ratio arriving at Earth [12]. In 2008-2011, IceCube has announced three showering events characteristic of ν_e's or ν_τ's (or their antiparticles, since non-magnetized neutrino telescopes cannot distinguish ν from $\bar{\nu}$), in the energy range $\sim$1–2 PeV, in addition to another 34 events with energies between 30 TeV and 300 TeV. At 5.7σ, a purely atmospheric neutrino background explanation of these events is rejected.

For a given propagation distance L, the flavor state $|\nu_\alpha\rangle$ evolves into $|\nu_\alpha(L)\rangle = \sum_k e^{-iE_kL} U^*_{\alpha k} |\nu_k\rangle$. The transition probability from the flavor state $|\nu_\alpha(L)\rangle$ to $|\nu_\beta\rangle$ is then given by $P_{\alpha\beta} = |\langle\nu_\beta|\nu_\alpha(L)\rangle|^2$ for any α and β taken from the set $\{e, \mu, \tau\}$. For cosmic neutrinos, the characteristic distance is much larger than the oscillation length, motivating a statistical average over a neutrino ensemble. This averaging randomizes a quantum-mechanical phase $\phi_{jk} \equiv L(m_j^2 - m_k^2)/2E$ between states such that the phase factor $e^{i\phi_{jk}}$ averages to zero (think of wrapping a complex number of unit modulus around zero in its complex plane). The result is a reduction of P to $\langle P\rangle \equiv \mathscr{P}$, where the brackets connote the averaging of all phase factors to zero. The matrix elements of the reduced propagation matrix $\mathscr{P}$ are simple, positive definite elements:

$$\mathscr{P}_{\alpha\beta} = \sum_j |U_{\alpha j}|^2 |U_{\beta j}|^2 = \left(|U|^2 \left(|U|^2 \right)^T \right)_{\alpha\beta}, \tag{V.1}$$

and the matrix elements of $|U|^2$ are defined to be $|U_{\alpha\beta}|^2$. Expressions for the elements

$\mathscr{P}_{\alpha\beta}$ in terms of the PDG set $\{\theta_{32},\ \theta_{12},\ \theta_{13},\ \delta\}$, are given in Ref. [21]. It is this $\langle P\rangle = \mathscr{P}$ matrix that propagates the flavor ratios injected at the source, $\vec{W} = (W_e, W_\mu, W_\tau)$ with normalization $W_e + W_\mu + W_\tau = 1$, to the flavor ratios observed on Earth, $\vec{w} = (w_e, w_\mu, w_\tau)$ with mormalization $w_e + w_\mu + w_\tau = 1$, i.e. $\vec{w} = \mathscr{P}\vec{W}$.

The outline for this chapter is: In §(V.2) we discuss the TriBiMaximal (TBM) matrix, and additional perturbations that are needed to agree with experiment. We argue that the TBM matrix offers a $\mathscr{P}$ matrix that is qualitatively good, but not good in the details warranted by some observables. One feature of $\mathscr{P}_{\rm TBM}$ that will turn out to be significant is the vanishing determinant. With a vanishing determinant, one cannot invert the propagation to infer the cosmic flavor ratios from the measured, Earthly ones. We present the restrictions on the flavor propagation matrix $\mathscr{P}$ that result from unitarity of the PMNS leptonic mixing matrix. In §(V.3) we present the concept of flavor triangles at Earth as a concise way to indicate the result of flavor decoherence arising from propagation of neutrinos over cosmic distances. Some illustrative examples of $\mathscr{P}$ matrix and their associated Earthly triangles are given. In §(V.4) we expand on the idea that just as the constraint $w_e + w_\mu + w_\tau = 1$ reduces a Euclidian volume octant to a triangular surface, so will another constraint reduces the triangle to a line. We give four physically motivated examples of such constraints, the first two involving properties of the propagation matrix (equivalently, constraints from or on the mixing angles), the third involving Earthly detector efficiencies, and the fourth involving particle physics at the sources. Our first example, that of a vanishing determinant of $\mathscr{P}$, is presented in §(V.4.1). The TBM ansätz gives a vanishing determinant. Since TBM is known phenomenologically to be nearly true, the true determinant cannot be far from zero. We show that it can be zero, and that the breaking of the ν_μ-ν_τ symmetry does not necessarily imply a non-vanishing Det($\mathscr{P}$). We discuss implications for ν_μ-ν_τ symmetry, the cornerstone of the TBM ansätz. We derive the unique value of δ that simultaneously allows for vanishing Det($\mathscr{P}$) and broken ν_μ-ν_τ symmetry. Finally, we prove a theorem that the area of the Earthly flavor triangle and the determinant of $\mathscr{P}$ are directly proportional,

with proportionality constant $\sqrt{3}/2$. This theorem therefore tells us that any nonzero area for the Earthly triangle implies an invertible $\mathscr{P}$, which in turn implies the possibility of reconstructing the flavor ratios at injection directly from the ratios measured at Earth. In §(V.4.2) we present our second example of "constraint" that evokes a straight line solution for the Earthly flavors, namely, the conditions for a triangle that is so thin that it is experimentally indistinguishable from a straight-line solution. It turns out that the width of the triangle projected onto the w_μ-w_τ-axis, which is zero with good ν_μ-ν_τ symmetry, is second order in the standard angle-phase parameter $\theta_{13}\cos\delta$ and second order in the deviation of the θ_{32} from its TBM value of $\pi/4$. Since experiment tells us that both of these parameters are small, their squares are very small, and we understand the thinness of the Earthly triangle. In §(V.4.3) we discuss the ambiguities presented by the ν_τ events. At energies $\lesssim$ PeV, the ν_τ events look like showers. At energies $\gtrsim 10$ PeV, the double-bang nature of the ν_τ events leads to a combination of shower, track and identifiably ν_τ events. We consider the simplified case for $E_\nu \lesssim$ PeV, where only two event topologies of "flavor" are resolved in Earthly detectors, namely "tracks" and "showers". This simplification then becomes our third example of a constraint which reduces the flavor triangle to a line. We assess the statistical significance of the flavor inferences of this model, for the case of 140 total events and an injection ratio of (1:2:0). The 140 event sample is the typical expectation for 10 years of IceCube running, or 1-2 years of running for IceCube's proposed, large-volume extension, Gen2. The statistical limitations on the determination of $\vec{w}$ are significant. In §(V.4.4) we discuss the constraint that results from assuming that the injection of ν_τ's is negligibly small, as is expected in all popular models. Although the Earthly triangle may have a nonzero area from considerations of the $\mathscr{P}$ matrix, the "no ν_τ injection" constraint reduces the Earthly possibility to just a boundary line of the Earthly triangle. Differentiation of this boundary line from the thin flavor triangle requires a considerable set of statistics (events). Such an event collection may not be achievable in the near future. Our conclusions are collected in §(V.5).

V.2 Perturbations About TBM Values, and Flavor Triangles

With the TBM model, the U matrix, the $|U|^2$ and $\mathscr{P}$ matrices, are

$$U_{\rm TBM} = \frac{1}{\sqrt{6}} \begin{pmatrix} 2 & \sqrt{2} & 0 \\ -1 & \sqrt{2} & \sqrt{3} \\ -1 & \sqrt{2} & -\sqrt{3} \end{pmatrix}, \quad |U|^2_{\rm TBM} = \frac{1}{6} \begin{pmatrix} 4 & 2 & 0 \\ 1 & 2 & 3 \\ 1 & 2 & 3 \end{pmatrix},$$
$$\mathscr{P}_{\rm TBM} = \frac{1}{18} \begin{pmatrix} 10 & 4 & 4 \\ 4 & 7 & 7 \\ 4 & 7 & 7 \end{pmatrix}. \tag{V.2}$$

Two ingredients of the TBM ansätz that are necessary to realize the ν_μ-ν_τ symmetry are that $\theta_{13} = 0$, forcing U_{e3} to be zero, and that θ_{32} is maximal, equal to $\frac{\pi}{4}$. However, the DAYA-BAY experiment in China [31] has inferred a nonzero $\sin^2(2\theta_{13}) = 0.092 \pm 0.016\,(\text{stat.}) \pm 0.005\,(\text{syst.})$, and and the RENO experiment in Korea [32] has $\sin^2(2\theta_{13}) = 0.113 \pm 0.013\,(\text{stat.}) \pm 0.019\,(\text{syst.})$, each at 68% C.L. These values of $\sin^2(2\theta_{13})$ give a θ_{13} that is more than 10σ removed from zero, indicating that the TBM model is not valid. Indeed, cosmic neutrinos can be used as a probe of broken ν_μ-ν_τ symmetry [41].

In 3D space, the allowed area of the flavor fractions at injection is an equilateral hyper-triangle, with vertices at $(1,0,0)$, $(0,1,0)$, and $(0,0,1)$ in the Euclidean W_e–W_μ–W_τ space. The allowed Earthly fractions, with unitary constraint $w_e + w_\mu + w_\tau = 1$, constitute a flavor triangle defined by the three vertices at $\mathscr{P}\,(1,0,0)^{\rm T}$, $\mathscr{P}\,(0,1,0)^{\rm T}$, and $\mathscr{P}\,(0,0,1)^{\rm T}$. The unitary and symmetric properties of $\mathscr{P}$ matrix are encapsulated in writing:

$$\mathscr{P} = \begin{pmatrix} 1-(a+b) & a & b \\ a & 1-(a+c) & c \\ b & c & 1-(b+c) \end{pmatrix} = \frac{1}{18} \begin{pmatrix} 10 & 4 & 4 \\ 4 & 7 & 7 \\ 4 & 7 & 7 \end{pmatrix} + \frac{1}{18} \Delta\mathscr{P}, \tag{V.3}$$

where the upper bound on the off-diagonal, flavor-changing probabilities $\mathscr{P}_{\alpha\beta}$ is $\frac{1}{2}$ from

the two-flavor oscillation limit, and the well-known lower bound on the diagonal matrix elements $\mathscr{P}_{\alpha\alpha}$ for the three-flavor system is $\frac{1}{3}$; these limits lead directly to $0 \leq a,\ b,\ c \leq \frac{1}{2}$, and the pairwise range $0 \leq a+b,\ b+c,\ c+a \leq \frac{2}{3}$.[1]

Here, $\Delta\mathscr{P}$ is the perturbation over the TBM matrix. The expansion of $\Delta\mathscr{P}$ to second order in the deviations of the three leptonic mixing angles from their TBM values can be found in [77]. There it was derived that

$$\Delta\mathscr{P} = A \begin{pmatrix} 4 & -2 & -2 \\ -2 & 1 & 1 \\ -2 & 1 & 1 \end{pmatrix} + B \begin{pmatrix} 0 & 1 & -1 \\ 1 & -1 & 0 \\ -1 & 0 & 1 \end{pmatrix} + C \begin{pmatrix} 0 & 0 & 0 \\ 0 & 1 & -1 \\ 0 & -1 & 1 \end{pmatrix}, \quad \text{(V.4)}$$

where A, B and C are calculated functions of the deviations of mixing parameters from the TBM values. A does not depend on δ, and in the best-fit case [48] is equal to -0.154; B ranges over $[-0.003, -0.842]$ as $\cos\delta$ ranges over $[-1, 1]$; C is quadratic in the deviation, to lowest order (A and B each contain a linear dependence), and ranges over $[0.073, 0.319]$. We note that the perturbations to the TBM matrix are much smaller than the elements of the TBM matrix: The A-correction is at most 8%, the B-correction is at most 20%, and the C-correction is at most 5%. Thus, the TBM ordering $\mathscr{P}_{ee} > \{\mathscr{P}_{\mu\mu},\ \mathscr{P}_{\mu\tau},\ \mathscr{P}_{\tau\tau}\} > \{\mathscr{P}_{e\mu},\ \mathscr{P}_{e\tau}\}$ (i.e., $1 > a+b+c$, and $c > a$ or b) is maintained in the real world. This ordering result will be an important ingredient in establishing a conclusion in §(V.4.4.2). We have shown that the TBM matrix is a good approximation, and in much of what follows we adopt this approximation. However, it has a vanishing determinant, and so cannot serve as an approximation for discussions that require a non-vanishing determinant.

[1] We note that unitarity relations were recently presented in detail in [76]. Our simple constraints here are equivalent to two of the three unitarity results obtained there. Their third constraint, that twice any element of the set $\{a,b,c\}$ plus either one of the remaining two elements is bounded by $\frac{25}{24}$ (for example, that $2a+b \leq \frac{25}{24}$), is neither reproduced nor needed here.

V.3 The Flavor Triangle at Earth

It is clear that nonzero $a,\ b,\ c$, i.e. neutrino flavor mixing, reduce the size of the Earthly triangle relative to the original injection triangle.

V.3.1 The Centroid Point

The centroid of the Earthly triangle is at the point $(\frac{1}{3},\ \frac{1}{3},\ \frac{1}{3})$, as shown in Fig. V.1. It can be achieved by symmetric mixing, $a = b = c = \frac{1}{3}$, which further implies the democratic matrix with all elements equal to $\frac{1}{3}$:

$$\mathscr{P}_{\frac{1}{3}} = \frac{1}{3}\begin{pmatrix} 1 & 1 & 1 \\ 1 & 1 & 1 \\ 1 & 1 & 1 \end{pmatrix}. \tag{V.5}$$

Unitarity guarantees that any injection vector $\vec{W}$ will return the centroid point at Earth when propagated by $\mathscr{P}_{\frac{1}{3}}$. The Determinant of $\mathscr{P}_{\frac{1}{3}}$ vanishes, so $\mathscr{P}_{\frac{1}{3}}$ is not invertible; while all input vectors $\vec{W}$ will lead to an Earthly (1:1:1) ratio were this propagation matrix to be correct, the converse is not true – an Earthly (1:1:1) ratio does not imply the correctness of this propagation matrix. A common counter-example is the input vector resulting from charged-pion decays that $\vec{W} = \frac{1}{3}$(1:2:0), which leads to $\frac{1}{3}$(1:1:1) if a propagation matrix close to the TBM matrix, given in Eq. (V.2), is assumed.

We find that all Earthly triangles determined by arbitrary $\theta_{32},\ \theta_{21}$, and the pair $(\theta_{13},\ \delta_{\rm CP})$, include the centroid point. The reason is simple: the unitarity constraint guarantees that the big injection triangle and small Earthly triangle share the same centroid. Of course, restrictions on the initial values of the $\vec{W}$ flavor components may restrict the Earthly triangle to an area that does not contain the centroid. An example of such a restriction is the common assumption that little or no ν_τ's are produced at the source, i.e., that W_τ is effectively zero. We discuss the implications of this assumption in a later section.

V.3.2 Example: Quark Mixing

It is well known that the quark mixing angles are much smaller than those of the neutrino sector. Hence, we expect the analog of quark flavor mixing to offer an Earthly triangle much more similar to the unmixed source triangle. In Fig. V.1, we visualize the smallness of the quark mixing angles by plotting the reduction of the hadronic source triangle to what would be the Earthly triangle if quarks were to oscillate (they don't, as they are confined, and their mass differences are very large). The corners of the Earthly matrix are given by $\mathscr{P}$-propagation of the unmixed flavor vectors (1,0,0), (0,1,0), and (0,0,1). As we discuss later, the quark triangle after mixing is about 80% in area of the original unmixed triangle.

V.4 One More Constraint Reduces the Triangle to a Line – Four Examples

Since the unitarity constraint $\omega_e + \omega_\mu + \omega_\tau = 1$ reduces a 3D volume to a 2D hyper surface (in this case, to our flavor triangle), it is not surprising that a further constraint would reduce the 2D triangle to a 1D line. We can think of four possible, interesting constraints, each of which would affect the dimensional reduction. The first is a vanishing determinant of $\mathscr{P}$. The second is that the triangle is so "thin" that no experiment will be able to differentiate the thin triangle from a straight line, say, the line determining either of the thin triangle's longer borders. The third is that in first approximation, a neutrino telescope can distinguish only between track and shower events at neutrino energies $\lesssim 1$ PeV or $\gtrsim 10$ PeV, and not among all three neutrino flavors. And the fourth is the probably true statement that the sources do not emit any significant amount of ν_τ's, i.e. "no-ν_τ injected". Of course, if two of these conditions hold, then the two lines will in general intersect in a point within the triangle, and the flavor ratios at Earth will be determined. In general, three of these conditions cannot hold simultaneously, unless they are linearly dependent.

The first two conditions, if true, result from properties of the $\mathscr{P}$ matrix. The third condition results from a property of the detectors, their efficiency to identify "double-bang" ν_τ events [46]. And the final, fourth condition results from a property of the source, the

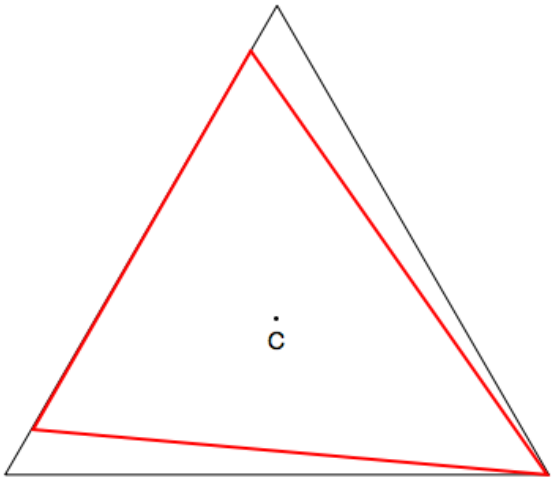

Figure V.1: The analog of the Earthly triangle is shown (red interior triangle) for the mixing angles that relate quark flavors and masses. Also shown is the centroid point, labelled "C".

presence or absence of a significant nonzero W_τ.

There may also be new neutrino physics [78; 6], such as mixing with sterile neutrinos, of new neutrino interactions, but we consider these possibilities to be less motivated and less measurable in the flavor ratios.

In the following sections, we consider, one at a time, all four possible conditions. Since the Earthly triangle, once let loose subject to only unitarity, must contain the centroid point, the first two conditions, studied in sections (V.4.1) and (V.4.2), will create a (one-dimensional) line through the centroid, but rotated in the plane relative to the vertical TBM line. This rotation angle may be thought of as a measure of ν_μ-ν_τ symmetry breaking. The third condition, studied in section (V.4.3), will reduce the Earthly triangle to a boundary line of the triangle, the line connecting the vectors $\mathscr{P}\,(1,0,0)^{\mathrm{T}}$ and $\mathscr{P}\,(0,1,0)^{\mathrm{T}}$. This line is again rotated with respect to the vertical TBM line, but this time without passing through the centroid point. The fourth possible condition, described and analyzed in section (V.4.4), reduces Earthly measurements to just two even topologies, w_{track} and w_{shower}.

V.4.1 Extra Constraint – First Example: A Vanishing Determinant

An important, possible use of the $\mathscr{P}$ matrix is to use it to evolve backwards the observed neutrino flavor ratio at Earth to obtain the ratios injected at the sources. The injection ratios then reveal the nature of source dynamics [16; 5].

For a given neutrino flavor vector $\vec{W} \equiv (W_e, W_\mu, W_\tau)$ injected at cosmic sources, the corresponding flavor vector $\vec{w} \equiv (w_e, w_\mu, w_\tau)$ measured at Earth is given by $\vec{w} = \mathscr{P}\vec{W}$. If $\mathscr{P}$ has a non-vanishing determinant and hence is an invertible matrix, then the inverse equation

$$\vec{W} = \mathscr{P}^{-1}\,\vec{w} \tag{V.6}$$

allows one to use the neutrino flavor ratios observed at Earth to determine those dynamically injected at cosmic sources [7]. From Eq. (V.1) we get that the determinant of the propagation matrix $\mathscr{P}$ is given by

$$\mathrm{Det}(\mathscr{P}) = \mathrm{Det}\left(|U|^2 \cdot (|U|^2)^T\right) = \left(\mathrm{Det}\left(|U|^2\right)\right)^2 . \tag{V.7}$$

Inversion of the $\mathscr{P}$ matrix was not viable with the TBM ansätz for neutrino mixing, because the nature of the ν_μ-ν_τ symmetry assumed for the matrix was expressed as identical second and third rows up to phases (± 1) [79]. This implies identical second and third rows for the $|U|^2$ matrix, and therefore a vanishing determinant. Since the determinant of $\mathscr{P}$ is equal to the squared determinant of $|U|^2$ (as given in Eq. (V.7)), with the TBM ansätz, $\mathscr{P}$ has a vanishing determinant and is therefore not invertible.

Backwards evolution, as spelled out in Eq. (V.6), requires that the matrix $\mathscr{P}$ be invertible, i.e., have a nonzero determinant. However, if the ν_μ-ν_τ symmetry were exact, the determinant of the $\mathscr{P}$ matrix would vanish. We now know that θ_{13} is nonzero. A common belief is that nonzero θ_{13} implies that the ν_μ-ν_τ symmetry is broken. However, utilizing the PDG form of the PMNS lepton-mixing matrix, we may conclude that ν_μ-ν_τ symmetry arises from the following conditions [23]: (i) $\theta_{32} = \frac{\pi}{4}$, as in the TBM ansätz, and (ii)

$\sin 2\theta_{21} \sin\theta_{13} \cos\delta = 0$. Given that inferences from neutrino oscillation experiments are that $\theta_{13} \neq 0$ and $\theta_{21} \neq \frac{\pi}{2}$, the only remaining possibility for exact ν_μ-ν_τ symmetry is that $\theta_{32} = \frac{\pi}{4}$, and $\delta = \pm\pi/2$. Although the restriction of δ to $\pm\frac{\pi}{2}$ is not part of the TBM ansätz, this particular value $\delta = \pm\frac{\pi}{2}$ is presently viable.[2] Nevertheless, it seems probable at present that ν_μ-ν_τ symmetry is broken.

Even so, a point which we choose to emphasize is that broken ν_μ-ν_τ symmetry does not imply that the determinant for $\mathscr{P}$ is non-vanishing. One of the major points we explore in this work is the possibility of having a vanishing determinant for $\mathscr{P}$ even if the ν_μ-ν_τ symmetry is broken.

V.4.1.1 Det($\mathscr{P}$), Vanishing or Not?

According to Eq. (V.7), to study the vanishing of Det($\mathscr{P}$), it is enough to analyze the vanishing of Det($|U|^2$). In linear algebra, Det($|U|^2$) = 0 means that the three rows of $|U|^2$ (or columns, since $|U|^2 \to (|U|^2)^{\mathrm{T}}$ leaves the determinant invariant) are linearly-dependent [81]. Explicitly, one has the three equations

$$\alpha\,|U_{ej}|^2 + \beta\,|U_{\mu j}|^2 + \gamma |U_{\tau j}|^2 = 0 \quad \text{for } j = 1,\ 2,\ 3\,, \tag{V.8}$$

where at least two of the three constants α, β, γ are nonzero.

A trivial solution to Eq. (V.8) is the ν_μ-ν_τ symmetry, for which we have

$$\alpha = 0, \quad \beta = 1, \quad \gamma = -1\,. \tag{V.9}$$

With this ν_μ-ν_τ symmetry, one will always get the same flavor ratios at Earth for ν_μ and ν_τ, regardless of the flavor ratios at cosmic sources; the Earthly "triangle" collapses to the vertical line bisecting the w_μ and w_τ coordinates.

[2] In a recent data fit [80], slightly favored values of δ are $\pm\pi/2$. However, all values of δ are presently permissible at 2σ range.

V.4.1.2 Broken ν_μ-ν_τ Symmetry and Vanishing Det($\mathscr{P}$)

With the help of unitary conditions and linear algebra simplifications, we find

$$\mathrm{Det}\left(|U|^2\right) = \begin{vmatrix} 1 & 1 & 3 \\ |U_{\mu 1}|^2 - |U_{\tau 1}|^2 & |U_{\mu 2}|^2 - |U_{\tau 2}|^2 & 0 \\ |U_{\tau 1}|^2 & |U_{\tau 2}|^2 & 1 \end{vmatrix} . \tag{V.10}$$

From this simplified expression, we can readily obtain

$$\mathrm{Det}\left(|U|^2\right) = \cos 2\theta_{13} \cos 2\theta_{21} \cos 2\theta_{32} - \frac{1}{2} \sin 2\theta_{21} \sin 2\theta_{32} (1 - 3\sin^2\theta_{13}) \sin\theta_{13} \cos\delta \tag{V.11}$$

As a check, we see that this expression vanishes under exact ν_μ-ν_τ symmetry, which requires $\sin 2\theta_{21} \sin\theta_{13} \cos\delta = 0$ and $\theta_{32} = \frac{\pi}{4}$. What we now point out that is new, is that a vanishing determinant is also viable even when the ν_μ-ν_τ symmetry is broken. Setting the determinant in Eq. (V.11) to zero, we solve for the CP-violating phase δ as determined by the three mixing angles. We find that Det($|U|^2$) vanishes, and therefore Det($\mathscr{P}$) vanishes, if

$$\cos\delta = 2\cot 2\theta_{32} \cot 2\theta_{21} \cot 2\theta_{13} \left(\frac{2\cos\theta_{13}}{1 - 3\sin^2\theta_{13}} \right) . \tag{V.12}$$

With the recent global best fit data [48; 80; 1] one can easily find that the RHS of Eq. (V.12) ranges from -0.92 to 0.91 as the mixing angles vary in the 2σ range, which corresponds to the ranges for δ of $\pm[24.5^\circ, 156.9^\circ]$. Currently, the Dirac CP-violating phase is still largely unconstrained at a 2σ level. Should terrestrial experiments in the future infer a δ satisfying Eq. (V.12), then Det($\mathscr{P}$) vanishes and the inverse propagation matrix $\mathscr{P}^{-1}$ needed to evolve the observed neutrino flavor ratio backwards to their injection ratios at cosmic sources does not exist.

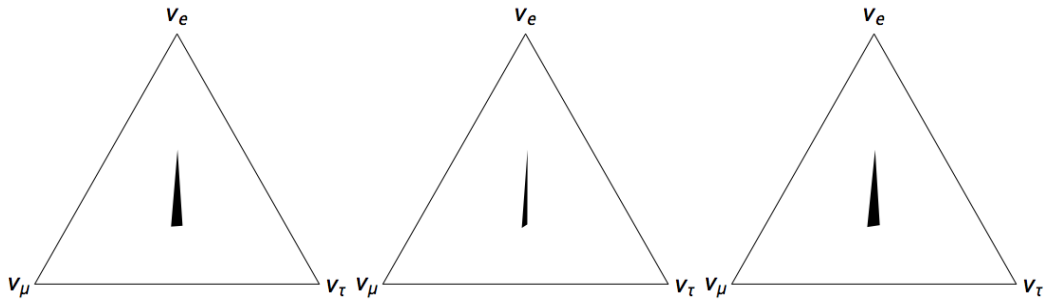

Figure V.2: The Earthly triangles for the best values of, from left to right, the Normal Hierarchy with θ_{32} in first octant, Normal Hierarchy with θ_{32} in second octet, and the Inverted Hierarchy.

V.4.1.3 A Theorem Relating the Area of the Earthly Triangle and Det($\mathscr{P}$)

In this section, we present and prove an interesting theorem that relates the determinant of the $\mathscr{P}$ matrix to the area of the allowed flavor triangle on Earth. In 3D space, the allowed area of the original flavor triangle is $\frac{\sqrt{3}}{2}$. The equilateral hyper-triangle results from the single unitary constraint, $W_e + W_\mu + W_\tau = 1$, on infinite 3D Euclidean space. After mixing, the area S of the Earthly flavor ratio triangle with the three vertices given by $\mathscr{P}\,(1,0,0)^{\mathrm{T}}$, $\mathscr{P}\,(0,1,0)^{\mathrm{T}}$, and $\mathscr{P}\,(0,0,1)^{\mathrm{T}}$, is much smaller than the area ($\frac{\sqrt{3}}{2}$) of the original source triangle. Interestingly, we find that the area of this Earthly triangle, denoted by S, is proportional to the absolute value of the determinant of the $\mathscr{P}$ matrix. Simply stated, the theorem says that

$$\text{THEOREM}: \qquad S = \frac{\sqrt{3}}{2}\,|\mathrm{Det}(\mathscr{P})|\,. \tag{V.13}$$

In terms of the three independent off-diagonal elements of $\mathscr{P}$ defined in Eq. (V.3), we have

$$\mathrm{Det}(\mathscr{P}) = 1 - 2(a+b+c) + 3(ab+ac+bc). \tag{V.14}$$

Also in terms of these three independent parameters, the coordinates of the three vertices of the Earthly triangle are $(1-a-b,\, a,\, b)$, $(a,\, 1-a-c,\, c)$, and $(b,\, c,\, 1-b-c)$. Taking the difference of these three vectors defines the vector lengths of the three sides of the Earthly

triangle. And from the lengths of the three sides, we calculate the triangle's area, S. A bit of algebra leads to $\sqrt{3}/2$ times the expression in Eq. (V.14). The theorem is proven.

An interesting case is the area of the quark-flavor triangle after mixing. Inputing the quark sector values $a = 9.65\%$, $b = 0.017\%$, and $c = 0.33\%$, we get for the area $A_{\text{mixed}} = 80.1\%$ times the unmixed (original) area of $\sqrt{3}/2$. Very little contraction of the triangle's area has occurred, due to very little mixing. The situation is very different with the large mixing angles in the neutrino sector, as we shall see.

Illuminating checks result for the TBM model, where the ν_μ-ν_τ symmetry (which implies a vanishing determinant) leads to an Earthly flavor ratio located on the $w_\mu = w_\tau$ symmetry line; and for the even simpler case of the democratic propagation matrix, $\mathscr{P}_{\frac{1}{3}}$, where the two constraints of the exact ν_e-ν_μ-ν_τ symmetry (again implying a vanishing determinant) lead to a single point at the centroid of the injection triangle. In both of the above cases, the area of the region occupied by the Earthly triangle is zero.

V.4.2 Extra Constraint – Second Example: Thinness of the Earthly Triangle

The difference between the vertices of the Earthly triangle which are closest to each other, i.e. the points $\mathscr{P}(0,\ 1,\ 0)^{\mathrm{T}}$ and $\mathscr{P}(0,\ 0,\ 1)^{\mathrm{T}}$, projected onto the $w_e = 0$ axis of the triangle, is

$$\Delta W(w_e = 0) = 2 - (a + b + 4c)\,. \tag{V.15}$$

This final expression turns out to be 2/9 times the parameter "C" of Ref. [77], where it was shown that C is second order in deviation of the standard angle-phase parameters $\theta_{13}\cos\delta$ and θ_{32} from their respective TBM values of zero and $\frac{\pi}{4}$, and independent of θ_{21}. Thus we learn that the small deviations from TBM will appear as an even smaller deviation of the Earthly triangle from the straight line of the TBM model. Furthermore, the long sides of the Earthly triangle will in general be slightly rotated with respect to the vertical TBM line (by small angles that are second order in θ_{13} and $(\theta_{32} - \frac{\pi}{4})$). Examples of the thinness of the Earthly triangle, and its rotation, are shown in Fig. V.2 for the best fit values of the Normal

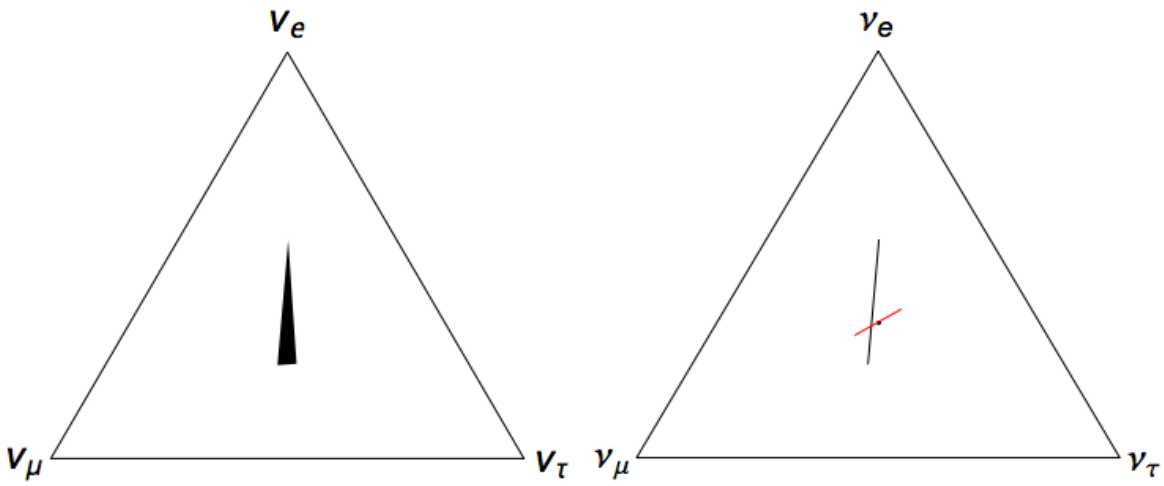

Figure V.3: The left panel shows the flavor triangle at Earth, for the best fit values of the Normal Hierarchy with θ_{32} in the first octant (also shown in the previous Fig. V.2), and the right panel shows the straight line that results from the assumption that ν_τ production at the source is negligible. Note that the "no-ν_τ injected" line is a boundary of the full triangle, and therefore does not contain the centroid (shown) at the point $(\frac{1}{3}, \frac{1}{3}, \frac{1}{3})$. The small red line is the 2σ statistical error at the centroid values, assuming 140 total events. We note that the statistical error bar is comparable to the width of the Earthly triangle, shown in the left panel.

Hierarchy with θ_{32} lying in the first and second octants, and for the Inverted Hierarchy. The example of the best-fit values for the Normal Hierarchy with θ_{32} in the first octant is shown again in Fig. V.3. In particular, the fraction of original triangular area given by the Earthly triangle ranges from a maximum of 1.2% at $\delta = 0$, to zero for the vanishing determinant value discussed above. The ability of an experiment to measure the width of the Earthly triangle thus requires a very good accuracy, of order $(\Delta W(w_e = 0))$, as given above.

V.4.3 Extra Constraint – Third Example: ν_τ Confusion, and Statistical Error

V.4.3.1 Tau Neutrino Interaction Topologies, and Ambiguity

The mean free decay length of the tau in vacuum (i.e. $c\times$lifetime) is $L_\tau = \frac{1}{4}\,(E_\tau/5\,\mathrm{PeV})$ km, and so some tau track lengths may be visible (leading to so-called "double-bang" events) in the energy decade centered on ~ 5 PeV in IceCube, and at somewhat higher energy in the proposed larger, sparser, IceCube-Gen2 [82]. We pose our discussion on the IceCube

configuration of optical modules. Below about 1 PeV, the tau decays promptly, and so its decay shower contributes the initial ν_τ shower. The event then adds to the "shower" class of events, like the ν_e. Well above about 10 PeV, the ν_τ shower and the tau decay shower are well separated, so much so that both showers do not appear in the detector. If the ν_τ shower appears in the detector (with $\sim 20\%$ of the initial neutrino energy), then it is followed by a track, adding to the "track" event class, like the charged-current ν_μ events. If the tau shower appears in the detector, it is preceded by a track, in which case the event is identifiable as a ν_τ-initiated event. The isolation of event types depends very much on the particular detector's configuration, its efficiency for separation of events in classes, and the energy of the initial neutrino. Accordingly, the pigeon-holing of event types is bet left to the experimenters. Here we analyze just the simple case of lower energy events, $\lesssim$ PeV, where the the showering fraction $w_{\rm shower}$ is identified with the sum $w_e + w_\tau$, and the track fraction $w_{\rm track}$ is identified with the w_μ. (We neglect neutral currents, since they contribute a lower-energy shower, which is negligible for a sufficiently falling energy-spectrum of initial neutrinos.) We remind the reader that the highest energy of neutrino events measured to date is only 2 PeV.

For our model calculation, the separation into ν_e and ν_τ events cannot be made. There are just two track topologies to consider, $w_{\rm track} = w_\mu$ and $w_{\rm shower} = w_e + w_\tau$, with $w_{\rm track} + w_{\rm shower} = 1$. There is a single parameter to be inferred from experiment, w_μ, or equivalently, $w_{\rm shower} = 1 - w_\mu$.

V.4.3.2 Statistical Error

One may ask what kind of statistical errors are expected from the measurement of a finite event number at Earth. To simplify the discussion we will assume that ν_e and ν_τ contribute only showering events, and ν_μ contributes only track events, i.e., we neglect the small contribution to shower events from ν_μ neutral-current interactions, and the contribution to track events from ν_τ events.

The statistical error will depend on the total number of events, N_{Total}, and on the measured number of track events (note that the measured number of shower events is related by $N_{\text{Total}} = N_{\text{track}} + N_{\text{shower}}$, where the experiment partitions the total number of events into "track" and "shower" events.) We begin with the definition $w^0_{\text{track}} = N_{\text{track}}/N_{\text{Total}}$, where the superscript "0" on w denotes the measured ratio. Then

$$\ln(w_{\text{track}}) = \ln(N_{\text{track}}) - \ln(N_{\text{track}} + N_{\text{shower}}), \quad \text{and therefore}$$

$$\delta \ln w^0_{\text{track}} = \frac{\delta w_{\text{track}}}{w^0_{\text{track}}} = \frac{1}{N_{\text{Total}}} \left(\delta N_{\text{track}} \left(\frac{N_{\text{shower}}}{N_{\text{track}}} \right) - \delta N_{\text{shower}} \right). \tag{V.16}$$

The two uncertainties, δN_{track} and δN_{shower}, are statistically uncorrelated, so we add them in quadrature. We also invoke the Poisson result that $\delta N_{\text{track}} = \sqrt{N_{\text{track}}}$ and $\delta N_{\text{shower}} = \sqrt{N_{\text{shower}}}$. Then a bit of algebra returns the relative error

$$\left| \frac{\delta w_{\text{track}}}{w^0_{\text{track}}} \right| = \sqrt{\frac{N_{\text{shower}}}{N_{\text{track}} N_{\text{Total}}}}, \tag{V.17}$$

and the absolute error

$$|\delta w_{\text{track}}| = \sqrt{\frac{N_{\text{track}} N_{\text{shower}}}{N^3_{\text{Total}}}} = \sqrt{\frac{w^0_{\text{track}} (1 - w^0_{\text{track}})}{N_{\text{Total}}}}. \tag{V.18}$$

The N_{track}-N_{shower} symmetry displayed in the middle result of Eq. (V.18) tells us that the errors in $|\delta w_{\text{track}}|$ and in $|\delta w_{\text{shower}}|$ are the same (i.e. that the two-dimensional error ellipse is in fact a circle.). Thus we may use the one d.o.f. formula (not surprising, since we have the constraint $w_{\text{track}} + w_{\text{shower}} = 1$) for the $m\sigma$ error contour:

$$\frac{(w_{\text{track}} - w^0_{\text{track}})^2}{\delta w^2_{\text{track}}} = m^2. \tag{V.19}$$

Finally we arrive at the final formula for the statistical error:

$$|w_{\rm track} - w^0_{\rm track}| = m \sqrt{\frac{w^0_{\rm track}\,(1 - w^0_{\rm track})}{N_{\rm Total}}}\,. \tag{V.20}$$

The factor $w^0_{\rm track}\,(1 - w^0_{\rm track})$ has a maximum of 1/4 at its symmetry point, $w^0_{\rm track} = 1/2$. In Fig. V.4 we plot this factor as a function of $w^0_{\rm track}$. In the figure, we have marked the symmetry point at $w_{\rm track} = 1/2$, and also the democratic, centroid value $w_{\rm track} = 1/3$.

In the right panel of Fig. V.3 we show with a small red line, the resulting 2σ error ($m = 2$, 95% CL) for the democratic value $w_{\rm track} = 1/3$. We show the error to lie along the bisector of the w_e-w_τ axis; in fact, the error is the same anywhere along the oblique line of constant w_μ. For the plot, we have taken $N_{\rm Total} = 140$ events, the number that would typically be collected by IceCube in ten years (~ 14 events per year), or the extension Gen2 in two years (~ 70 events per year). The value of the error is small, $\pm 2\sqrt{1/3 \times 2/3 \div 140} = \pm 0.080$. However, as seen in the figure, this statistical error is not small enough to allow differentiation of the Earthly flavor triangle's centroid and $W_\tau = 0$ boundary, nor to allow a clean inference of the Earthly triangle's width, at 95% CL. Of course, ten years of data collection by Gen2 will reduce the two-year error calculated here with a factor of $1/\sqrt{5} = 0.45$ or more.

The error for $w_{\rm shower}$ is the same as that for $w_{\rm track}$, but cannot be identified with a unique point in the flavor triangle since we have assumed here that w_e and w_τ are measured only in their summation: $w_e + w_\tau = w^0_{\rm shower} = 1 - w^0_{\rm track}$.

V.4.4 Extra Constraint – Fourth Example: No ν_τ's Produced at the Cosmic Source

Conventional dynamics at the neutrino sources will not produce many ν_τ's, because of the large mass of the leptonic partner particle, the τ ($m_\tau = 1.777$ GeV). D_s production and decay will result in a few ν_τ's, with the expectation of 0.1% for W_τ [21]. Setting W_τ to zero is a constraint, reducing the Earthly triangle to a straight line joining the points at $\mathscr{P}\,(1,0,0)^{\rm T}$ and $\mathscr{P}\,(0,1,0)^{\rm T}$. This line is an edge of the Earthly triangle obtained with arbitrary injec-

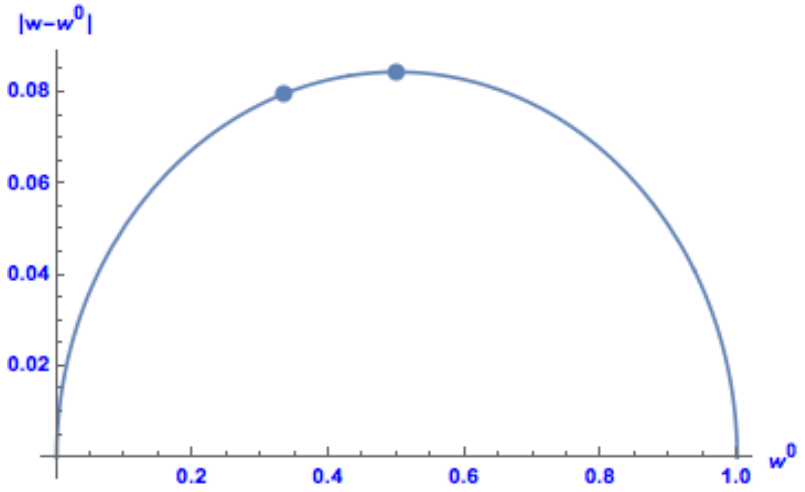

Figure V.4: The 2σ (m=2, 95% CL) standard deviation from Eq. (V.20) for $N_{\text{Total}} = 140$ events, versus the measured w^0 (the same for w_{track} and w_{shower}). The dots denote the special values of $w^0 = 1/2$ where the standard deviation has a maximum, and $w^0 = 1/3$, the centroid value expected for neutrino flavors from the pion decay chain.

tion models. As such, the line should not contain the Earthly triangle's centroid.

An interesting application of our "area theorem" is that at least one of the following popular arguments must be invalid:

(i) no ν_τ's are produced at the cosmic source;

(ii) $\text{Det}(\mathscr{P}) \neq 0$;

(iii) the flavor ratio at Earth is democratically $\frac{1}{3}$(1:1:1).

We note that the IceCube experiment claims compatibility of its data with the roughly democratic prediction from the pion decay-chain.

We construct the proof by showing that (iii) is invalid if (i) and (ii) are correct. Once this is proven, we are done: not all three statements may be correct.

According to Eq. (V.13), a non-vanishing determinant of the $\mathscr{P}$ matrix ((ii) above) guarantees that all the possible Earthly points occupy a small triangle with non-vanishing area. Moreover, with negligible ν_τ produced at cosmic sources [43] ((i) above), the small triangle is further reduced, to a straight line which connects the two points propagated from the vectors $\vec{W} = (1,0,0)$ and $\vec{W} = (0,1,0)$. Recall that the point $\frac{1}{3}$(1:1:1) is the centroid of

the small triangle. The centroid can never be a point on the boundary of the Earthly triangle, as it is an interior point. Thus it cannot be the Earthly point resulting from omission of ν_τ injection. Thus, our third argument (iii) is invalid.

Working backwards through the logic then leads to the inference that any observation of a strict democratic ratio on Earth would implicate either a vanishing determinant of $\mathscr{P}$, or some nonzero ν_τ production in the injection model. And to the inference that if the $\mathscr{P}$ matrix has a nonzero determinant, then any injection model with one or more flavors vanishing can never lead to a democratic ratio on Earth, since then the propagated point arriving at Earth must be located on the triangle's edge (boundary), which does not include the triangle's centroid.

V.4.4.1 Some Implications of Potential Flavor Measurements

As terrestrial experiments are making more precise measurements of the four leptonic mixing parameters, we can expect the accuracy of the $\mathscr{P}$ matrix to continually increase. Hence we may well determine the propagated Earthly triangle, and "no-ν_τ injected" boundary line, in the future [64; 83]. On the observational side, although the number of events expected in the near term by neutrino telescopes will not allow flavor analyses to determine the position of the flavor-ratio point at Earth (see, e.g. the statistical error bar presented in Fig. V.3), the point is determinable in the long term. Assuming statistically large future event samples, we infer an interesting and distinct result of each of the three possible locations of the flavor point with respect to the triangle:

- The measured Earthly point lies inside the Earthly triangle.

  In this case, the point is not on a boundary, and in particular is not on the "no-τ injected" boundary. So a significant amount of ν_τ must be emitted at the sources.

- The measured Earthly point lies on the "no-ν_τ injected" boundary.

  Then it is necessarily so that the sources do not emit a significant amount of ν_τ.

- The measured Earthly point lies outside the Earthly triangle.

  In this case, the implication is that some exotic physics must come into play. Examples of exotic physics include neutrino decay [62; 17; 84], active-sterile neutrino mixing [85], and new neutrino interactions [86; 87; 19; 88].

In fact the point in the Earthly flavor triangle characterizing flavor ratios is likely to be energy-dependent. It is beyond the scope of this work to deal with the extra complications that may result. When more flavor data is available, then it may be warranted to include these complicating options. For now the event sample is sufficient for only primitive flavor analyses.

V.4.4.2 Small but Nonzero W_τ

There are a priori six possible orderings of the three injection flavor ratios $\{W_e,\ W_\mu,\ W_\tau\}$ and of the three Earthly flavor ratios $\{w_e,\ w_\mu,\ w_\tau\}$. When the cosmic triangle is divided by the three bisectors, as shown in Fig. V.5, there results six symmetric sub-triangles. The six sub-triangles meet at the geometric centroid ($w_e = w_\mu = w_\tau = \frac{1}{3}$). Each bisector divides the ordering of two of the three W_α's or w_α's. Thus, there is a 1-1 correspondence between the orderings of the W_α's and w_α's, and the regions of the six sub-triangles. The correspondence is:

Sub-triangle 1: $W_\mu \geq W_\tau \geq W_e$ and $w_\mu \geq w_\tau \geq w_e$;

Sub-triangle 2: $W_\tau \geq W_\mu \geq W_e$ and $w_\tau \geq w_\mu \geq w_e$;

Sub-triangle 3: $W_\tau \geq W_e \geq W_\mu$ and $w_\tau \geq w_e \geq w_\mu$;

Sub-triangle 4: $W_e \geq W_\tau \geq W_\mu$ and $w_e \geq w_\tau \geq w_\mu$;

Sub-triangle 5: $W_e \geq W_\mu \geq W_\tau$ and $w_e \geq w_\mu \geq w_\tau$;

Sub-triangle 6: $W_\mu \geq W_e \geq W_\tau$ and $w_\mu \geq w_e \geq w_\tau$.

When $\mathrm{Det}(\mathscr{P}) \neq 0$, the Earthly triangle must have representation in each of the six sub-triangular regions, since the triangle must have a nonzero area and it must contain the centroid.

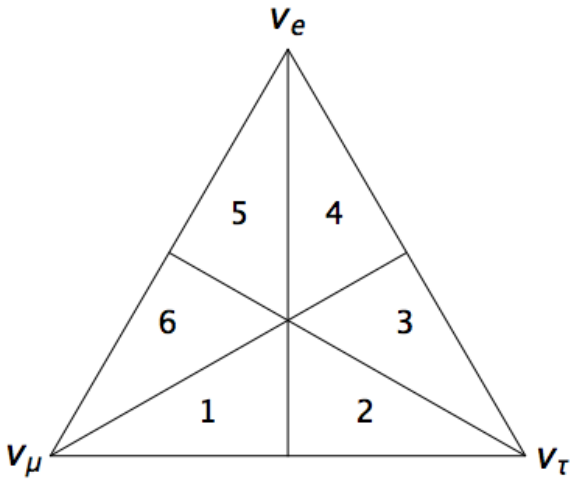

Figure V.5: Source triangle partitioned into six sub-triangles, each characterized by a distinct ordering of the injection ratios $\{W_e,\ W_\mu,\ W_\tau\}$, as well as the Earthly ratios $\{w_e,\ w_\mu,\ w_\tau\}$.

Popular injection models describe sources or processes that produce very little ν_τ i.e., $W_\tau < \{W_e, W_\mu\}$. Thus, there are only two popular orderings for the injection ratios: (i) $W_e > W_\mu > W_\tau$, and (ii) $W_\mu > W_e > W_\tau$. The first ordering is that of sub-triangle number 5; the second ordering is that of sub-triangle number 6.

We may ask whether any of these orderings would be preserved when the neutrinos are propagated to Earth. The answer is yes, the ordering $W_e > W_\mu$ (i.e., $W_\mu/W_e < 1$) is preserved at Earth, although the ordering $W_\mu > W_e$ (i.e., $W_\mu/W_e > 1$) need not be. Here is the proof:

from Eq. (V.3), we get

$$w_e - w_\mu = x\,(W_e - W_\tau) - y\,(W_\mu - W_\tau)\,, \tag{V.21}$$

where $x \equiv (1-2a-b)$, and $y \equiv (1-2a-c)$. Earlier we stated that $c > a$ or b, and that $1 > a+b+c$, even when the $\mathscr{P}$ matrix is perturbed about its TBM value. Thus, $x > y > 0$. Now assume that $W_e > W_\mu > W_\tau$. Then $(W_e - W_\tau) > (W_\mu - W_\tau) > 0$. Hence, the RHS of Eq. (V.21) is positive, and so the LHS must be positive, i.e., $w_e > w_\mu$, and the flavor

ordering is maintained. Next assume that $W_\mu > W_e > W_\tau$. Then the RHS is of indefinite sign, and therefore so is the LHS. Contrapositive argument infers that any Earthly point found inside sub-triangle 1, 2, or 6, must be due to an injection model with $W_\mu > W_e > W_\tau$ (corresponding to sub-triangle 6).

In fact, the W_μ/W_e ratio is readily measured at a neutrino telescope. In [7], a relation was derived for this ratio. Here we find that the relation may be simplified in form to

$$\frac{W_\mu}{W_e} = \frac{\mathscr{P}_{e\mu} - w_\mu}{w_\mu - \mathscr{P}_{\mu\mu}}. \tag{V.22}$$

The parameters $\mathscr{P}_{e\mu}$ and $\mathscr{P}_{\mu\mu}$ are determined from terrestrial measurements of mixing angles, as should be evident from this work. So just the parameter w_μ remains to be inferred from experiment. For neutrino energies $\lesssim$ PeV, the only track events are produced by the ν_μ charged current, and so Eq. (V.22) is readily determined. At a neutrino telescope such as IceCube, the fraction of ν_μ events incident at Earth w_μ is (neglecting the neutral-current contribution) also the fraction of track events. We emphasize that this result, and the derivation of it, remain valid independent of whether the determinant of $\mathscr{P}$ is vanishing or non-vanishing.

V.5 Conclusions

Flavor evolution of active neutrinos from distant astrophysical sources depends on the three mixing angles and one CP-violating phase, but in just three and not four independent CP-conserving combinations. This is because the large distance effectively averages over oscillation phases, reducing the quantum mechanical probability for flavor oscillation to a simpler classical mixing probability. This reduction entitles us to conveniently encapsulate the evolution in a symmetric 3 by 3 "flavor propagation matrix" $\mathscr{P} \equiv \langle P \rangle_{\text{phase averaging}}$. Unitarity of the PMNS leptonic mixing matrix implies certain restrictions on the $\mathscr{P}$ matrix. We have incorporated and explained these restrictions.

If the $\mathscr{P}$ matrix has nonzero determinant, then it may be inverted and the neutrino flavor

ratios at cosmic sources may be directly inferred from flavor ratios observed at Earth. A good approximation to the $\mathscr{P}$ matrix is the ν_μ-ν_τ symmetric TBM matrix $\mathscr{P}_{\rm TBM}$ with vanishing determinant. However, the form of the TBM matrix is known to be not strictly that of Nature, and so the question arises, "with ν_μ-ν_τ symmetry broken, can we conclude that Nature's $\mathscr{P}$ matrix has nonzero determinant and so is invertible?" We showed that the answer is negative. There is a unique value of δ, given in terms of the three angle parameters $\{\theta_{32},\ \theta_{12},\ \theta_{13}\}$, for which Det($\mathscr{P}$) is vanishing. If further experiments were to establish this value of δ as correct, then some new symmetry should be sought to enforce Det($\mathscr{P}$) $= 0$ for the neutrino sector.

Next we proved a theorem, that the determinant of $\mathscr{P}$ is proportional to the area of the Earthly flavor triangle. Thus, the inversion of $\mathscr{P}$ depends on the Earthly triangle having a nonzero area. The TBM version of $\mathscr{P}$ has a vanishing determinant and consequently, a vanishing area for its Earthly triangle. Thus, the small deviations of Nature's choices from the TBM values lead to a small nonzero area. We quantified this statement.

We then considered a simple model which allowed a straightforward calculation of statistical significance. The model was that ν_τ events contributed only to shower topologies in the detector, as would be expected for an event sample with energy up to $\sim$PeV. Thus, the origin of the shower events is the sum of ν_τ and ν_e events, while the origin of the track events is purely ν_μ. This model does not allow ν_e–ν_τ event separation, and so even idealized Earthly measurements within this paradigm cannot determine a point in the Earthly flavor triangle, but only a point on the line parameterized by $w_{\rm shower}$ and $w_{\rm track} = 1 - w_{\rm shower}$. We analyzed the dependence of the experimentally-determined point on the line on the event statistics. We established 2σ, 95% CL errors for an assumed 140 total events, a number expected to be typical of a decade of IceCube measurements, or a year or two of the IceCube extension Gen2. We found that the statistical error in this case to be comparable to the width of the Earthly triangle. Thus, separation of w_e from w_τ requires improved statistics. Above about a PeV, the topology of the ν_τ events becomes complicated, due to

the separation lengths between the resulting "double bangs" compared to the experiment's photo-detector separation length(s). The former lengths are stochastically distributed, and the mean separation length is energy-dependent. A three-flavor analysis under these conditions is beyond the scope of this work, and, in fact, best left to the experimenters.

The assumption that ν_τ's are not produced at the sources, i.e. that $W_\tau = 0$, is commonly believed to be true, due to the heavy mass of the tau particle associated with the ν_τ in charged–current production. Accordingly, we next considered the implications of the lack of significant ν_τ production at the source, by setting W_τ to zero. The condition $W_\tau = 0$ reduces the injection flavor triangle and the Earthly flavor triangle to straight lines on the boundaries of the would-be triangles. Whether the observed flavor point lies on the inside of the "no–ν_τ" boundary line, outside the line, or on the line leads to distinct physics conclusions, as we described. Even were ν_τ injection to be significant but less than that of ν_μ and ν_e, we showed that with Earthly flavor measurements, a test of source orderings $W_\mu > W_e > W_\tau$ versus $W_e > W_\mu > W_\tau$ becomes possible.

We conclude that although the Earthly flavor triangle is greatly reduced in area from the injection flavor triangle, it offers a powerful tool to elucidate at Earth some details of astrophysical neutrino injection.

BIBLIOGRAPHY

[1] Most recently updated at http://www.nu-fit.org/.

[2] Luis A. Anchordoqui, Vernon Barger, Ilias Cholis, Haim Goldberg, Dan Hooper, et al. Cosmic Neutrino Pevatrons: A Brand New Pathway to Astronomy, Astrophysics, and Particle Physics. *JHEAp*, 1-2:1–30, 2014.

[3] M.G. Aartsen et al. First observation of PeV-energy neutrinos with IceCube. *Phys.Rev.Lett.*, 111:021103, 2013.

[4] Lingjun Fu, Chiu Man Ho, and Thomas J. Weiler. Aspects of the Flavor Triangle for Cosmic Neutrino Propagation. *Phys. Rev.*, D91:053001, 2015.

[5] V. Barger, Lingjun Fu, J. G. Learned, D. Marfatia, S. Pakvasa, and T. J. Weiler. Glashow resonance as a window into cosmic neutrino sources. *Phys. Rev.*, D90:121301, 2014.

[6] Lingjun Fu and Chiu Man Ho. Flavor Ratios and Mass Hierarchy at Neutrino Telescopes. 2014.

[7] Lingjun Fu, Chiu Man Ho, and Thomas J. Weiler. Cosmic Neutrino Flavor Ratios with Broken $\nu_\mu - \nu_\tau$ Symmetry. *Phys. Lett.*, B718:558–565, 2012.

[8] D.J. Wagner and Thomas J. Weiler. Neutrino oscillations from cosmic sources: A nu window to cosmology. *Mod.Phys.Lett.*, A12:2497–2501, 1997.

[9] http://icecube.wisc.edu/.

[10] Homepage at http://antares.in2p3.fr/.

[11] Homepage at http://www.km3net.org/home.php.

[12] John F. Beacom, Nicole F. Bell, Dan Hooper, Sandip Pakvasa, and Thomas J. Weiler. Measuring flavor ratios of high-energy astrophysical neutrinos. *Phys.Rev.*, D68:093005, 2003.

[13] P.F. Harrison, D.H. Perkins, and W.G. Scott. Tri-bimaximal mixing and the neutrino oscillation data. *Phys.Lett.*, B530:167, 2002.

[14] Luis A. Anchordoqui, Haim Goldberg, Francis Halzen, and Thomas J. Weiler. Galactic point sources of TeV antineutrinos. *Phys.Lett.*, B593:42, 2004.

[15] Jorg P. Rachen and P. Meszaros. Photohadronic neutrinos from transients in astrophysical sources. *Phys.Rev.*, D58:123005, 1998.

[16] S. Hummer, M. Maltoni, W. Winter, and C. Yaguna. Energy dependent neutrino flavor ratios from cosmic accelerators on the Hillas plot. *Astropart.Phys.*, 34:205–224, 2010.

[17] John F. Beacom, Nicole F. Bell, Dan Hooper, Sandip Pakvasa, and Thomas J. Weiler. Decay of high-energy astrophysical neutrinos. *Phys.Rev.Lett.*, 90:181301, 2003.

[18] John F. Beacom, Nicole F. Bell, Dan Hooper, John G. Learned, Sandip Pakvasa, et al. PseudoDirac neutrinos: A Challenge for neutrino telescopes. *Phys.Rev.Lett.*, 92:011101, 2004.

[19] Irina Mocioiu and Warren Wright. Non-Standard Neutrino Interactions in the mu-tau sector. 2014.

[20] Paolo Lipari, Maurizio Lusignoli, and Davide Meloni. Flavor Composition and Energy Spectrum of Astrophysical Neutrinos. *Phys.Rev.*, D75:123005, 2007.

[21] Sandip Pakvasa, Werner Rodejohann, and Thomas J. Weiler. Flavor Ratios of Astrophysical Neutrinos: Implications for Precision Measurements. *JHEP*, 0802:005, 2008.

[22] J. Beringer et al. Review of Particle Physics (RPP). *Phys.Rev.*, D86:010001, 2012.

[23] Jiajun Liao, D. Marfatia, and K. Whisnant. Perturbations to μ-τ symmetry in neutrino mixing. *Phys.Rev.*, D87:013003, 2013.

[24] Zhi-zhong Xing. A Further study of $\mu - \tau$ symmetry breaking at neutrino telescopes after the Daya Bay and RENO measurements of θ_{13}. *Phys.Lett.*, B716:220–224, 2012.

[25] S.F. King. Parametrizing the lepton mixing matrix in terms of deviations from tribimaximal mixing. *Phys.Lett.*, B659:244–251, 2008.

[26] Davide Meloni and Tommy Ohlsson. Leptonic CP violation and mixing patterns at neutrino telescopes. *Phys.Rev.*, D86:067701, 2012.

[27] D.V. Forero, M. Tortola, and J.W.F. Valle. Global status of neutrino oscillation parameters after Neutrino-2012. *Phys.Rev.*, D86:073012, 2012.

[28] G.L. Fogli, E. Lisi, A. Marrone, D. Montanino, A. Palazzo, et al. Global analysis of neutrino masses, mixings and phases: entering the era of leptonic CP violation searches. *Phys.Rev.*, D86:013012, 2012.

[29] M.C. Gonzalez-Garcia, Michele Maltoni, Jordi Salvado, and Thomas Schwetz. Global fit to three neutrino mixing: critical look at present precision. *JHEP*, 1212:123, 2012.

[30] W. Grimus and P.O. Ludl. Correlations of the elements of the neutrino mass matrix. *JHEP*, 1212:117, 2012.

[31] F.P. An et al. Observation of electron-antineutrino disappearance at Daya Bay. *Phys.Rev.Lett.*, 108:171803, 2012.

[32] J.K. Ahn et al. Observation of Reactor Electron Antineutrino Disappearance in the RENO Experiment. *Phys.Rev.Lett.*, 108:191802, 2012.

[33] C. Adams et al. The Long-Baseline Neutrino Experiment: Exploring Fundamental Symmetries of the Universe. 2013.

[34] M.G. Aartsen et al. PINGU Sensitivity to the Neutrino Mass Hierarchy. 2013.

[35] Yu-Feng Li, Jun Cao, Yifang Wang, and Liang Zhan. Unambiguous Determination of the Neutrino Mass Hierarchy Using Reactor Neutrinos. *Phys.Rev.*, D88:013008, 2013.

[36] R.N. Cahn, D.A. Dwyer, S.J. Freedman, W.C. Haxton, R.W. Kadel, et al. White Paper: Measuring the Neutrino Mass Hierarchy. 2013.

[37] Mattias Blennow, Pilar Coloma, Patrick Huber, and Thomas Schwetz. Quantifying the sensitivity of oscillation experiments to the neutrino mass ordering. *JHEP*, 1403:028, 2014.

[38] Shao-Feng Ge, Kaoru Hagiwara, and Carsten Rott. A Novel Approach to Study Atmospheric Neutrino Oscillation. *JHEP*, 1406:150, 2014.

[39] Shao-Feng Ge and Kaoru Hagiwara. Physics Reach of Atmospheric Neutrino Measurements at PINGU. *JHEP*, 1409:024, 2014.

[40] M.G. Aartsen et al. Evidence for High-Energy Extraterrestrial Neutrinos at the IceCube Detector. *Science*, 342:1242856, 2013.

[41] Zhi-zhong Xing. Neutrino Telescopes as a Probe of Broken mu- tau Symmetry. *Phys.Rev.*, D74:013009, 2006.

[42] Sandhya Choubey and Werner Rodejohann. Flavor Composition of UHE Neutrinos at Source and at Neutrino Telescopes. *Phys.Rev.*, D80:113006, 2009.

[43] Eli Waxman and John N. Bahcall. High-energy neutrinos from cosmological gamma-ray burst fireballs. *Phys.Rev.Lett.*, 78:2292–2295, 1997.

[44] Zhi-Zhong Xing and Shun Zhou. Towards determination of the initial flavor composition of ultrahigh-energy neutrino fluxes with neutrino telescopes. *Phys.Rev.*, D74:013010, 2006.

[45] Raj Gandhi, Chris Quigg, Mary Hall Reno, and Ina Sarcevic. Ultrahigh-energy neutrino interactions. *Astropart.Phys.*, 5:81–110, 1996.

[46] John G. Learned and Sandip Pakvasa. Detecting tau-neutrino oscillations at PeV energies. *Astropart.Phys.*, 3:267–274, 1995.

[47] Reetanjali Moharana and Nayantara Gupta. Tracing Cosmic accelerators with Decaying Neutrons. *Phys.Rev.*, D82:023003, 2010.

[48] D.V. Forero, M. Tortola, and J.W.F. Valle. Neutrino oscillations refitted. 2014.

[49] Davide Meloni and Tommy Ohlsson. Neutrino flux ratios at neutrino telescopes: The Role of uncertainties of neutrino mixing parameters and applications to neutrino decay. *Phys.Rev.*, D75:125017, 2007.

[50] Arman Esmaili and Yasaman Farzan. An Analysis of Cosmic Neutrinos: Flavor Composition at Source and Neutrino Mixing Parameters. *Nucl.Phys.*, B821:197–214, 2009.

[51] K. Abe et al. The T2K Experiment. *Nucl.Instrum.Meth.*, A659:106–135, 2011.

[52] R.B. Patterson. The NOvA Experiment: Status and Outlook. *Nucl.Phys.Proc.Suppl.*, 235-236:151–157, 2013.

[53] A. Aguilar-Arevalo et al. Evidence for neutrino oscillations from the observation of anti-neutrino(electron) appearance in a anti-neutrino(muon) beam. *Phys.Rev.*, D64:112007, 2001.

[54] A.A. Aguilar-Arevalo et al. Improved Search for $\bar{\nu}_\mu \to \bar{\nu}_e$ Oscillations in the MiniBooNE Experiment. *Phys.Rev.Lett.*, 110:161801, 2013.

[55] P.A.R. Ade et al. Planck 2013 results. XVI. Cosmological parameters. *Astron.Astrophys.*, 571:A16, 2014.

[56] Chiu Man Ho and Robert J. Scherrer. Sterile Neutrinos and Light Dark Matter Save Each Other. *Phys.Rev.*, D87(6):065016, 2013.

[57] Steen Hannestad, Rasmus Sloth Hansen, and Thomas Tram. How Self-Interactions can Reconcile Sterile Neutrinos with Cosmology. *Phys.Rev.Lett.*, 112(3):031802, 2014.

[58] A. Donini, P. Hernandez, J. Lopez-Pavon, M. Maltoni, and T. Schwetz. The minimal 3+2 neutrino model versus oscillation anomalies. *JHEP*, 1207:161, 2012.

[59] Philipp Baerwald, Mauricio Bustamante, and Walter Winter. Neutrino Decays over Cosmological Distances and the Implications for Neutrino Telescopes. *JCAP*, 1210:020, 2012.

[60] Y. Farzan and A. Yu. Smirnov. Leptonic unitarity triangle and CP violation. *Phys.Rev.*, D65:113001, 2002.

[61] M.G. Aartsen et al. Observation of High-Energy Astrophysical Neutrinos in Three Years of IceCube Data. *Phys.Rev.Lett.*, 113:101101, 2014.

[62] Sandip Pakvasa, Anjan Joshipura, and Subhendra Mohanty. Explanation for the low flux of high energy astrophysical muon-neutrinos. *Phys.Rev.Lett.*, 110:171802, 2013.

[63] L. Dorame, O.G. Miranda, and J.W.F. Valle. Invisible decays of ultra-high energy neutrinos. 2013.

[64] Olga Mena, Sergio Palomares-Ruiz, and Aaron C. Vincent. Flavor Composition of the High-Energy Neutrino Events in IceCube. *Phys.Rev.Lett.*, 113:091103, 2014.

[65] Chien-Yi Chen, P.S. Bhupal Dev, and Amarjit Soni. Standard model explanation of the ultrahigh energy neutrino events at IceCube. *Phys.Rev.*, D89(3):033012, 2014.

[66] Arman Esmaili and Yasaman Farzan. Implications of the Pseudo-Dirac Scenario for Ultra High Energy Neutrinos from GRBs. *JCAP*, 1212:014, 2012.

[67] Sheldon L. Glashow. Resonant Scattering of Antineutrinos. *Phys.Rev.*, 118:316–317, 1960.

[68] Luis A. Anchordoqui, Haim Goldberg, Francis Halzen, and Thomas J. Weiler. Neutrinos as a diagnostic of high energy astrophysical processes. *Phys.Lett.*, B621:18–21, 2005.

[69] Atri Bhattacharya, Raj Gandhi, Werner Rodejohann, and Atsushi Watanabe. The Glashow resonance at IceCube: signatures, event rates and pp vs. $p\gamma$ interactions. *JCAP*, 1110:017, 2011.

[70] Raj Gandhi, Chris Quigg, Mary Hall Reno, and Ina Sarcevic. Neutrino interactions at ultrahigh-energies. *Phys.Rev.*, D58:093009, 1998.

[71] Luis A. Anchordoqui, Haim Goldberg, Morgan H. Lynch, Angela V. Olinto, Thomas C. Paul, et al. Pinning down the cosmic ray source mechanism with new IceCube data. *Phys.Rev.*, D89(8):083003, 2014.

[72] Gary J. Feldman and Robert D. Cousins. A Unified approach to the classical statistical analysis of small signals. *Phys.Rev.*, D57:3873–3889, 1998.

[73] L.A. Anchordoqui, V. Barger, H. Goldberg, J.G. Learned, D. Marfatia, et al. End of the cosmic neutrino energy spectrum. *Phys.Lett.*, B739:99–101, 2014.

[74] Lincoln Wolfenstein. Different Varieties of Massive Dirac Neutrinos. *Nucl.Phys.*, B186:147, 1981.

[75] Luis A. Anchordoqui, Thomas C. Paul, Luiz H. M. da Silva, Diego F. Torres, and Brian J. Vlcek. What IceCube data tell us about neutrino emission from star-forming galaxies (so far). *Phys.Rev.*, D89(12):127304, 2014.

[76] Xun-Jie Xu, Hong-Jian He, and Werner Rodejohann. Constraining Astrophysical Neutrino Flavor Composition from Leptonic Unitarity. 2014.

[77] Sandip Pakvasa, Werner Rodejohann, and Thomas J. Weiler. Unitary parametrization of perturbations to tribimaximal neutrino mixing. *Phys.Rev.Lett.*, 100:111801, 2008.

[78] Zhi-zhong Xing and Shun Zhou. Implications of Leptonic Unitarity Violation at Neutrino Telescopes. *Phys.Lett.*, B666:166–172, 2008.

[79] P.F. Harrison and W.G. Scott. mu - tau reflection symmetry in lepton mixing and neutrino oscillations. *Phys.Lett.*, B547:219–228, 2002.

[80] M.C. Gonzalez-Garcia, Michele Maltoni, and Thomas Schwetz. Updated fit to three neutrino mixing: status of leptonic CP violation. 2014.

[81] Steven J. Leon. *Linear Algebra with Applications*. Pearson, 8 edition, 2009.

[82] M. G. Aartsen et al. IceCube-Gen2: A Vision for the Future of Neutrino Astronomy in Antarctica. 2014.

[83] Sergio Palomares-Ruiz, Aaron C. Vincent, and Olga Mena. Spectral analysis of the high-energy IceCube neutrinos. *Phys. Rev.*, D91(10):103008, 2015.

[84] Jeffrey M. Berryman, Andre de Gouvea, and Daniel Hernandez. Solar Neutrinos and the Decaying Neutrino Hypothesis. 2014.

[85] Jeffrey M. Berryman, André de Gouvêa, Daniel Hernández, and Roberto L. N. Oliviera. Non-Unitary Neutrino Propagation. 2014.

[86] Kunihto Ioka and Kohta Murase. IceCube PeV-EeV neutrinos and secret interactions of neutrinos. *PTEP*, 2014(6):061E01, 2014.

[87] Tommy Ohlsson. A brief status of non-standard neutrino interactions. *Nucl.Phys.Proc.Suppl.*, 237-238:301–307, 2013.

[88] Kenny C. Y. Ng and John F. Beacom. Cosmic neutrino cascades from secret neutrino interactions. *Phys. Rev.*, D90(6):065035, 2014. [Erratum: Phys. Rev.D90,no.8,089904(2014)].